

MATRIX PRODUCT STATES
A Variational Approach to Strongly Correlated Systems

ANDREAS HALLER - AM RODELBERG 55 - 55131 MAINZ

Bachelor Thesis

Condensed Matter Theory - KOMET337
Institute of Physics

Johannes Gutenberg University Mainz



JOHANNES GUTENBERG
UNIVERSITÄT MAINZ

Matrix Product States, A Variational Approach to Strongly Correlated Systems

SUPERVISOR:

Junior Professor Matteo Rizzi, Ph.D.

COSUPERVISOR:

Junior Professor Román Orús, Ph.D.

LOCATION:

Mainz

TIME FRAME:

January 27 - April 7 2014

CONTENTS

1	INTRODUCTION	1
1.1	The Importance of Tensor Networks and Matrix Product States	1
2	THEORETICAL CONCEPTS	2
2.1	Review of Quantum Mechanics	2
2.2	Entanglement Quantification	4
2.3	Tensor Networks and Tensor Network Diagrams	6
2.4	The AKLT Matrix Product State	7
2.5	Matrix Product Operators	11
2.6	Generation of Canonical States	13
2.7	Iterative Search for Ground States	15
2.8	Building the effective Hamiltonian	18
2.9	Entanglement entropy, Correlations and Magnetisation	20
3	APPLICATION OF MPS TO PHYSICAL MODELS	22
3.1	The 1D Ising Model in a Transverse Field	22
3.1.1	Magnetisation	25
3.1.2	Correlations	26
3.1.3	Entropy	26
3.1.4	Conclusions and Perspective	27
3.2	Bilinear Biquadratic Spin-1 Chain	28
3.2.1	$\theta = \arctan(1/3)$ - The AKLT Point	29
3.2.2	$\theta = 0$ - The Heisenberg Point	30
3.2.3	$\theta = -\pi/2$ - The Klümper Point	31
3.2.4	Entanglement Spectrum at different Phase Points	31
4	SUMMARY AND OUTLOOK	33

A	APPENDIX A - PROGRAMME CODE	34
A.1	AKLT Model	34
A.2	Variational Approach	37
B	APPENDIX B - MATHEMATICAL TOOLS	41
B.1	Schmidt Decomposition	41
B.2	QR Decomposition	42
C	APPENDIX C - MISCELLANEOUS	43
C.1	The Ising Model and its Majorana Form	43
C.2	Additional Plots	45
c.2.1	Ising Model	45
C.3	AKLT Model	47
C.4	Heisenberg Model	48
	Listings	50
	BIBLIOGRAPHY	51

ACRONYMS

AKLT	Affleck, Lieb, Kennedy and Tasaki
BLBQ	bilinear-biquadratic
DMRG	density matrix renormalisation group
EPR	Einstein-Podolsky-Rosen
MPO	matrix product operator
MPS	matrix product state
OBC	open boundary condition
PBC	periodic boundary condition
QRD	QR decomposition
SVD	singular value decomposition
SSVD	sequential singular value decomposition
TN	tensor network

INTRODUCTION

1.1 THE IMPORTANCE OF TENSOR NETWORKS AND MATRIX PRODUCT STATES

Quantum many-body systems, in particular strongly correlated systems within condensed matter physics, are of extraordinary importance for modern physics: They can describe a variety of systems with highly interesting properties, e.g. spin glasses [16], frustrated magnets [18] or superconductors [3], just to name a few. The huge number of interacting degrees of freedom even for simple models of these systems is posing a challenge to both, analytical and numerical solution approaches. The dimension of the underlying Hilbert space grows exponentially with the number of particles in a system. If it can be described by differential systems on a symplectic manifold, and if there are as many constant of motion as degrees of freedom one is able to solve it analytically and the system is called "integrable" [5]. But still the large majority of such models are not integrable, and therefore have to be treated with numerical techniques. As numerical approaches to determine the eigenvalues and eigenvectors of a Hamiltonian scale disproportionate to the number of particles or total system length, only small systems could be analysed with the computing power typically available today using "brute force" diagonalisation methods. Fortunately, most physical systems can be sufficiently described by focusing on *local* interactions, which locate the important physical ground states in a very small portion of the huge Hilbert space.

For such a system, the matrix product state (MPS) formalism turns out to be a mighty variational approach to rebuild the ground states at zero temperature with a small amount of processing power. It is equivalent to a parametrisation of a more compact submanifold of the Hilbert space, describing only the sectors with reduced entanglement between the system's subparts by construction. The interesting states are those with low energy portions of the spectrum and a few excited thermal states. It has been proven [6], that ground and thermal states of Hamiltonians with local interactions obey the area law for entanglement, which immediately connects the low energy states to those with low entanglement. The intense interest in MPS in the last few years is based on the power of the density matrix renormalisation group (DMRG) method, which has been developed by S. White et al. in the 1990's [20].

The main intention of this thesis is to provide an introduction into tensor networks and the reformulated DMRG as part of the MPS formalism under a quantum information perspective. A DMRG programme will be implemented and tested for the Ising and bilinear-biquadratic (BLBQ) Heisenberg model by a comparison of numerical results to analytical solutions - as far as they exist.

THEORETICAL CONCEPTS

To introduce in the formalism of MPS, we will proceed as follows: Basics of quantum mechanics will be reviewed in order to become familiar with the definition of entanglement. The next section gives an insight in how to quantify entanglement, i.e. how to measure entanglement in a quantum mechanical system. After that, the basics of tensor networks will be provided in order to introduce the graphical representation for MPS. A short section about the Affleck, Lieb, Kennedy and Tasaki (AKLT) model is sufficient to understand a simple MPS. The main intention of the next part is to provide the basics for the implementation of a DMRG algorithm, reformulated in the MPS language. A few lines about measuring observables with the MPS obtained by the DMRG programme is a crossover to the demonstration chapter.

2.1 REVIEW OF QUANTUM MECHANICS

In quantum mechanics, information is stored in the system's wave function $|\psi\rangle \in \mathcal{H}$. \mathcal{H} is called *Hilbert space* and $|\psi\rangle$ is a vector with complex coefficients. An example is given by a two level system (e.g. spin-1/2),

$$|\psi\rangle = \alpha |\uparrow\rangle + \beta |\downarrow\rangle, \text{ where } \{|\uparrow\rangle, |\downarrow\rangle\} \text{ is a basis of } \mathcal{H} \subseteq \mathcal{C}^2. \quad (2.1)$$

This is called a *ket*. One also defines a *bra* via $\langle\psi| = \alpha^* \langle\uparrow| + \beta^* \langle\downarrow|$. The two level systems define a *qu(antum)bit*, if $|\uparrow\rangle \equiv |0\rangle$ and $|\downarrow\rangle \equiv |1\rangle$. Then the state $|\psi\rangle = \alpha |0\rangle + \beta |1\rangle$ is a superposition of 0's and 1's. The scalar product of two states is defined

$$\begin{aligned} |\psi\rangle &= \alpha |0\rangle + \beta |1\rangle, |\phi\rangle = \tilde{\alpha} |0\rangle + \tilde{\beta} |1\rangle \\ \Rightarrow \langle\phi|\psi\rangle &= \tilde{\alpha}^* \cdot \alpha + \tilde{\beta}^* \cdot \beta. \end{aligned} \quad (2.2)$$

Physical states are normalised $\langle\psi|\psi\rangle = |\alpha|^2 + |\beta|^2 = 1$. Given a quantum state $|x\rangle$, the probability P of the system $|\psi\rangle$ being in the state $|x\rangle$ is given by $P(|x\rangle) = |\langle x|\psi\rangle|^2$. If one is making a measurement of a defined state, the whole system will collapse, e.g.

$$\begin{aligned} |\psi\rangle &= \alpha |0\rangle + \beta |1\rangle \\ \xrightarrow[\text{leads to}]{\text{measuring } \sigma_z} +1} &\Leftrightarrow |\psi\rangle = |0\rangle. \end{aligned} \quad (2.3)$$

A collapse is a *non-unitary* operation. Physical operations (apart from measurements) are represented by *unitary operators*.

$$\begin{aligned} U \text{ is unitary} &\Leftrightarrow UU^\dagger = U^\dagger U = \mathbb{1} \\ U^\dagger &\equiv (U^\top)^* = (U^*)^\top \end{aligned} \quad (2.4)$$

The well-known Pauli matrices are a good example for unitary operators:

$$\sigma_x = \begin{pmatrix} 0 & 1 \\ 1 & 0 \end{pmatrix}, \quad \sigma_y = \begin{pmatrix} 0 & -i \\ i & 0 \end{pmatrix}, \quad \sigma_z = \begin{pmatrix} 1 & 0 \\ 0 & -1 \end{pmatrix}. \quad (2.5)$$

Pauli matrices have the following properties:

$$\{\sigma_i, \sigma_j\} = 2\delta_{ij}, \quad [\sigma_i, \sigma_j] = 2i \sum_{k=1}^3 \epsilon_{ijk} \sigma_k. \quad (2.6)$$

Unitary operations preserve the norm of a state. For $|\psi'\rangle = U|\psi\rangle$,

$$\langle \psi' | \psi' \rangle = \langle U\psi | U\psi \rangle = \langle \psi | U^\dagger U | \psi \rangle = \langle \psi | \psi \rangle. \quad (2.7)$$

This implicitly means, that the probability is always conserved ($\sum P_i = 1$). Composite systems are described by tensor products of Hilbert spaces

$$|\psi_1\rangle \in \mathcal{H}_1, |\psi_2\rangle \in \mathcal{H}_2, \text{ composite system } |\psi_3\rangle \in \mathcal{H}_3 = \mathcal{H}_1 \otimes \mathcal{H}_2. \quad (2.8)$$

In terms of basis states, e.g. qubits

$$\begin{aligned} \{|0\rangle_1, |1\rangle_1\} &\in \mathcal{H}_1 & \{|0\rangle_1 \otimes |0\rangle_2, |1\rangle_1 \otimes |1\rangle_2, |0\rangle_1 \otimes |1\rangle_2, |1\rangle_1 \otimes |0\rangle_2\} &\in \mathcal{H}_3, \\ \{|0\rangle_2, |1\rangle_2\} &\in \mathcal{H}_2 \\ \dim(\mathcal{H}_1) = \dim(\mathcal{H}_2) = 2, \dim(\mathcal{H}_3) &= \dim(\mathcal{H}_1) \cdot \dim(\mathcal{H}_2) = 4. \end{aligned} \quad (2.9)$$

Therefore, some possible states for $|\psi_3\rangle$ are:

$$|\psi_3\rangle = \begin{cases} |0\rangle_1 \otimes |1\rangle_2, \\ \frac{1}{\sqrt{2}} (|0\rangle_1 \otimes |0\rangle_2 + |0\rangle_1 \otimes |1\rangle_2) \equiv |0\rangle_1 |+\rangle_2, \quad |+\rangle = \frac{1}{\sqrt{2}} (|0\rangle + |1\rangle), \\ \frac{1}{2} (|0\rangle_1 \otimes |0\rangle_2 - |0\rangle_1 \otimes |1\rangle_2 - |1\rangle_1 \otimes |0\rangle_2 + |1\rangle_1 \otimes |1\rangle_2), \\ \frac{1}{\sqrt{2}} (|0\rangle_1 \otimes |0\rangle_2 + |1\rangle_1 \otimes |1\rangle_2). \end{cases} \quad (2.10)$$

Whenever a state is not described by a product of states of the corresponding subsystems, the system is called *entangled*. Otherwise it is called *separable*.

$$\begin{aligned} |\psi\rangle \in \mathcal{H}_1 \otimes \mathcal{H}_2 \text{ is entangled iff.} \\ \nexists |\psi_i\rangle \in \mathcal{H}_i \Rightarrow |\psi\rangle = |\psi_1\rangle \otimes |\psi_2\rangle \end{aligned} \quad (2.11)$$

Examples for separable and entangled states are:

$$|\psi\rangle = \begin{cases} |0,0\rangle \rightarrow \text{separable}, \\ \frac{1}{2} (|0,0\rangle + |0,1\rangle + |1,0\rangle + |1,1\rangle) = |+,+\rangle \rightarrow \text{separable}, \\ \frac{1}{\sqrt{2}} (|0,0\rangle + |1,1\rangle) \equiv |\Phi^+\rangle \rightarrow \text{entangled}, \\ \frac{1}{\sqrt{2}} (|1,0\rangle - |0,1\rangle) \equiv |\Psi^-\rangle \rightarrow \text{entangled}. \end{cases} \quad (2.12)$$

Entangled states can be understood as a distance independent correlation, which is called the Einstein-Podolsky-Rosen (EPR) paradox. To illustrate this idea, imagine one creates a $|\psi^-\rangle$ state, sends one qubit to Darmstadt and keeps the other in Mainz.

A measurement of spin-"0" in Mainz will result in an immediate collapse¹ of the qubit in Darmstadt to $|1\rangle$. Entanglement is a non-local property of $|\psi\rangle$. Therefore, it does not change under local unitary operators, e.g. $E(|\psi_{1,2}\rangle) = E(U_1 \otimes U_2 |\psi_{1,2}\rangle)$, where U_1, U_2 are unitary operators [15].

Note

Entanglement, as in the above definition, appears to be a bipartite property. But it can also be multipartite, e.g. one can have $|\psi\rangle \in \mathcal{H}_{1,2,3} = \mathcal{H}_1 \otimes \mathcal{H}_2 \otimes \mathcal{H}_3$ with $|\psi\rangle \neq |\psi_1\rangle \otimes |\psi_2\rangle \otimes |\psi_3\rangle$. To exclude pairwise entanglement, one should also demand that $|\psi\rangle \neq \{|\psi_{1,2}\rangle \otimes |\psi_3\rangle, |\psi_1\rangle \otimes |\psi_{2,3}\rangle\}$. Therefore, entanglement properties of a quantum state may be very subtle, and a full classification of entangled states is only possible in particular cases.

2.2 ENTANGLEMENT QUANTIFICATION

As it turns out [9], the van Neumann entropy is a "good" entanglement quantity for pure bipartite systems. In order to understand the definition given at the end of this section, the introduction of a few mathematical tools is necessary.

Theorem: Singular Value Decomposition (SVD)²

For every matrix M of dimensions $(d_A \times d_B)$ exists a singular value decomposition (SVD) such that

$$M = U\Lambda V^\dagger, \quad (2.13)$$

with the following properties:

- U has dimensions $(d_A \times \min(d_A, d_B))$ and orthonormal columns. $U^\dagger U = \mathbb{1}$ (if $d_A \leq d_B$) and $UU^\dagger = \mathbb{1}$
- Λ has dimensions $(\min(d_A, d_B) \times \min(d_A, d_B))$ and is diagonal with non-negative entries λ_α . The number of non-zero singular values m is the so called Schmidt rank of M .
- V^\dagger has dimensions $(\min(d_A, d_B) \times d_B)$ and orthonormal rows. $V^\dagger V = \mathbb{1}$ (if $d_A \geq d_B$) and $VV^\dagger = \mathbb{1}$.

Theorem: Schmidt Decomposition

Let

$$|\psi_{A,B}\rangle \in \mathcal{H}_A \otimes \mathcal{H}_B, \quad |\psi_{A,B}\rangle = \sum_{i,j} \psi_{i,j} |i\rangle_A |j\rangle_B. \quad (2.14)$$

¹ But there is no information transmitted, if one does not allow a classical bit communicating the outcome in Mainz to the scientist in Darmstadt - no information is transmitted for free!

² A proof can be found in [11].

There exists always a so called Schmidt decomposition

$$|\psi_{A,B}\rangle = \sum_{\alpha}^m \lambda_{\alpha} |\alpha\rangle_A |\alpha\rangle_B , \quad (2.15)$$

with $m \leq \min(\dim(\mathcal{H}_A), \dim(\mathcal{H}_B))$ and $\langle\alpha|\alpha'\rangle_A = \langle\alpha|\alpha'\rangle_B = \delta_{\alpha\alpha'}$. This means there is a orthonormal basis of \mathcal{H}_A and \mathcal{H}_B , which is a direct consequence of the singular value decomposition. A proof can be found in chapter B.1.

1. $|\alpha\rangle_A, |\alpha\rangle_B$ are called *Schmidt vectors*.
2. $m = 1 \Leftrightarrow |\psi_{A,B}\rangle$ is separable.
3. m is called *Schmidt rank* and provides a first measure of entanglement. The larger m is, the more entangled is the state.

The entropy can be measured by decomposition of the state either via SVD to read out the singular values, which directly refer to the entanglement of the bond between the two subsystems, or equivalently by calculating the reduced density matrix. The reduced density matrix of a state with common orthonormal basis $|\psi\rangle$ of two systems A and B is defined as the partial trace of the common density matrix $\rho_{AB} = \rho_A \otimes \rho_B$,

$$\rho_{A/B} \equiv \text{tr}_{B/A}(\rho_{AB}) . \quad (2.16)$$

This can be simplified using the Schmidt decomposition to

$$\rho_A = \sum_{\alpha=1}^r \lambda_{\alpha}^2 |\alpha\rangle_A \langle\alpha|_A , \quad \rho_B = \sum_{\alpha=1}^r \lambda_{\alpha}^2 |\alpha\rangle_B \langle\alpha|_B . \quad (2.17)$$

The von Neumann entropy is then computed from reduced density matrix $\rho_{A/B}$

$$\begin{aligned} S_{A/B} &\equiv -\text{tr}(\rho_{A/B} \log(\rho_{A/B})) \\ &= -\sum_{\alpha}^r \lambda_{\alpha}^2 \log(\lambda_{\alpha}^2) . \end{aligned} \quad (2.18)$$

If we consider the singlet state of two spin-1/2, $|\psi^{-}\rangle = \frac{1}{\sqrt{2}}(|\uparrow\downarrow\rangle - |\downarrow\uparrow\rangle)$, the total state can be written in matrix form

$$\begin{aligned} |\psi\rangle &= \sum_{a,b} \Sigma_{a,b} |ab\rangle \quad a, b \in \{\uparrow, \downarrow\} , \text{ with} \\ \Sigma &= \frac{1}{\sqrt{2}} \begin{pmatrix} 0 & 1 \\ -1 & 0 \end{pmatrix} . \end{aligned} \quad (2.19)$$

A readout of the entanglement spectrum is obtainable via SVD

$$\begin{aligned} \Sigma &= U\Lambda V^{\dagger} = \frac{1}{\sqrt{2}} \begin{pmatrix} 0 & 1 \\ 1 & 0 \end{pmatrix} \begin{pmatrix} 1 & 0 \\ 0 & 1 \end{pmatrix} \begin{pmatrix} -1 & 0 \\ 0 & 1 \end{pmatrix} \\ &\Rightarrow -\Lambda^2 \log(\Lambda^2) = \begin{pmatrix} 0.5 & 0 \\ 0 & 0.5 \end{pmatrix} \\ &\Rightarrow S = +1 , \end{aligned} \quad (2.20)$$

which is the maximum entanglement entropy for this system. For a separable state, e.g. $|\psi\rangle = \frac{1}{\sqrt{4}}(|\uparrow\rangle + |\downarrow\rangle)^2$, the expression becomes

$$\Sigma = \frac{1}{\sqrt{4}} \begin{pmatrix} 1 & 1 \\ 1 & 1 \end{pmatrix} = U\Lambda V^\dagger = \frac{1}{\sqrt{4}} \begin{pmatrix} -1 & -1 \\ -1 & 1 \end{pmatrix} \begin{pmatrix} 1 & 0 \\ 0 & 0 \end{pmatrix} \begin{pmatrix} -1 & -1 \\ -1 & 1 \end{pmatrix}, \quad (2.21)$$

which yields a von Neumann entropy $S = 0$.

2.3 TENSOR NETWORKS AND TENSOR NETWORK DIAGRAMS

A *tensor* is a composed system of complex numbers in multidimensional arrays. Its *rank* is defined as the number of indices. Hence, a single number x is a tensor of rank zero, a vector x_α of rank one, the Kronecker delta δ_{il} of rank two, and the Levi-Civita tensor ϵ_{ijk} of rank three. To introduce *tensor networks* and *tensor network contractions*, it is usual to define a graphical representation for tensors (see Fig. 1).



Figure 1: Examples for a graphical representation of tensors. From left to right: Scalar, vector, matrix, rank-3 tensor. Each index is represented by a tensor leg.

Tensor contractions are sums over one or more equal indices of different tensors.

$$C_{\alpha\gamma} = \sum_{\beta=1}^D A_{\alpha\beta} B_{\beta\gamma} \quad (2.22)$$

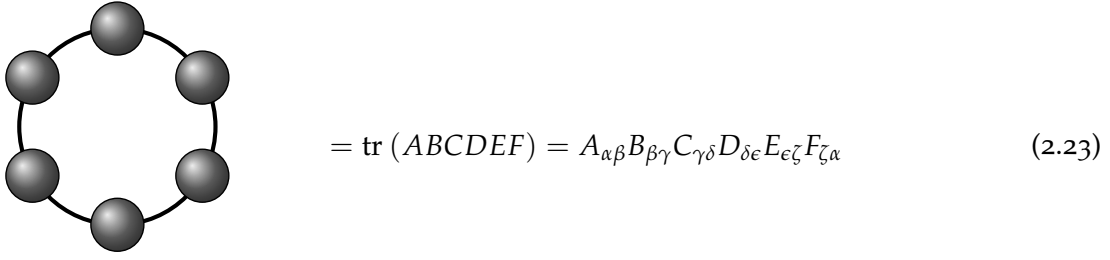
Eq. 2.22 is an example for a contraction of index β . The non-contracted indices α and γ are called *open indices*. These conventions yield a graphical representation for contractions. Hence figure 2 is a matrix multiplication in equivalence to Eq. 2.22.



Figure 2: Graphical representation of contraction 2.22.

This notation makes a complex contraction visual and points out some properties that are hidden in the huge amount of indices, e.g. the cyclic property of a trace of a matrix product (see Fig. 3). Consider the matrix multiplication of Eq. 2.22 and assume A and B are $(m \times m)$ matrices, the total number of operations for this contraction is $\mathcal{O}(m^3)$. This amount of operations cannot be reduced using naive approaches for matrix multiplications³, but in the case of more complex tensor contractions, it is important to think about the sequential arrangement. For example, the result of both contractions

³ The Strassen algorithm reduces $\mathcal{O}(m^{\log_2(8)}) \rightarrow \mathcal{O}(m^{\log_2(7)})$.



$$= \text{tr} (ABCDEF) = A_{\alpha\beta} B_{\beta\gamma} C_{\gamma\delta} D_{\delta\epsilon} E_{\epsilon\zeta} F_{\zeta\alpha} \quad (2.23)$$

Figure 3: Trace of a matrix product in graphical and analytical notation with sum convention.

in Fig. 4 is the same, but they need a different number of operations. This is essential for programming the contraction in order to find the optimised computation time [10].

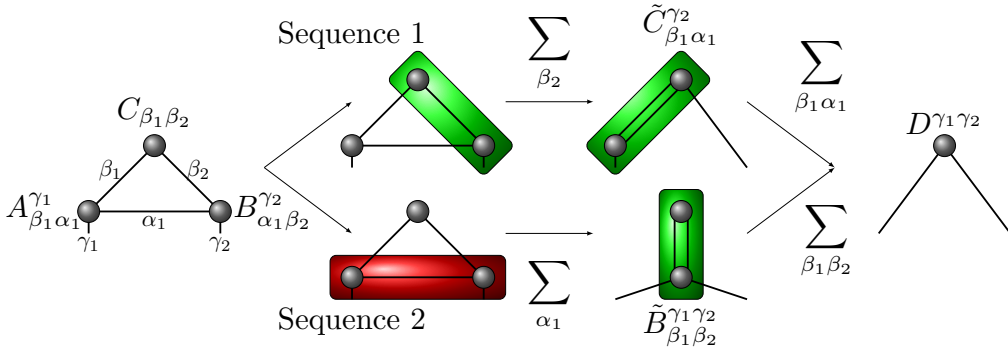


Figure 4: Assume that each leg has dimension m . Green contractions include $\mathcal{O}(m^4)$ operations and the red one $\mathcal{O}(m^5)$. Therefore, sequence 1 is the better choice.

2.4 THE AKLT MATRIX PRODUCT STATE

For a short review about the principles and the physical understanding of MPS, a very nice example can be given by the valence-bond-states as part of the AKLT model.

Consider the Hamiltonian

$$H = \sum_{l=1}^B \alpha (\vec{S}_l \vec{S}_{l+1}) + \beta (\vec{S}_l \vec{S}_{l+1})^2 \quad \text{and} \quad \alpha = 1, \quad \beta = \frac{1}{3} \quad (2.24)$$

for a 1D spin-1 chain with length L . $B = L - 1$ for an open boundary condition (OBC) and $B = L$ for a periodic boundary condition (PBC), where $L + 1 \equiv 1$. Each particle may occupy one of three orthonormal states $|\sigma\rangle \in \{|+\rangle, |0\rangle, |-\rangle\}$. The spin operators can be written component by component $\vec{S}_l = (S_l^x, S_l^y, S_l^z)^T$,

$$S_l^j = \underbrace{\mathbb{1} \otimes \mathbb{1} \otimes \dots}_{l-1} \otimes S^j \otimes \underbrace{\mathbb{1} \dots \otimes \mathbb{1}}_{L-l} \quad j \in \{x, y, z\}, \quad (2.25)$$

with their explicit forms

$$S^x = \frac{1}{\sqrt{2}} \begin{pmatrix} 0 & 1 & 0 \\ 1 & 0 & 1 \\ 0 & 1 & 0 \end{pmatrix}, \quad S^y = \frac{1}{\sqrt{2}} \begin{pmatrix} 0 & -i & 0 \\ i & 0 & -i \\ 0 & i & 0 \end{pmatrix}, \quad S^z = \begin{pmatrix} 1 & 0 & 0 \\ 0 & 0 & 0 \\ 0 & 0 & -1 \end{pmatrix}. \quad (2.26)$$

Each term of the Hamiltonian in Eq. 2.24 has the form

$$H_{\text{obc},l} = (\vec{S}_A \cdot \vec{S}_B) + \frac{1}{3}(\vec{S}_A \cdot \vec{S}_B)^2, \quad (2.27)$$

which can be simplified to

$$\begin{aligned} S_A S_B &= \frac{1}{2} ((S_A + S_B)^2 - (S_A^2 + S_B^2)) = \frac{1}{2} (S_{\text{tot}}^2 - 4) \\ &= \frac{1}{2} \cdot \begin{cases} 0 - 4 & s_{\text{tot}} = 0 \\ 2 - 4 & s_{\text{tot}} = 1 \\ 6 - 4 & s_{\text{tot}} = 2 \end{cases} \\ \Rightarrow H_{\text{obc},l} &= -\frac{2}{3} (P_0 + P_1) + \frac{4}{3} P_2 = -\frac{2}{3} \mathbb{1} + 2P_2, \end{aligned} \quad (2.28)$$

with the spin projection operators P_s . For OBC, the ground state of H_l is four-fold degenerate with the states

$$\begin{aligned} |1, +1\rangle &= \frac{1}{\sqrt{2}} (|+\rangle_l |0\rangle_{l+1} - |0\rangle_l |+\rangle_{l+1}), \\ |1, 0\rangle &= \frac{1}{\sqrt{2}} (|+\rangle_l |-\rangle_{l+1} - |-\rangle_l |+\rangle_{l+1}), \\ |1, -1\rangle &= \frac{1}{\sqrt{2}} (|-\rangle_l |0\rangle_{l+1} - |0\rangle_l |-\rangle_{l+1}), \\ |0, 0\rangle &= \frac{1}{\sqrt{3}} (|+\rangle_l |-\rangle_{l+1} + |-\rangle_l |+\rangle_{l+1} - |0\rangle_l |0\rangle_{l+1}). \end{aligned} \quad (2.29)$$

The three triplet states are given by

$$|+\rangle = |\uparrow\uparrow\rangle, \quad |0\rangle = \frac{1}{\sqrt{2}} (|\uparrow\downarrow\rangle + |\downarrow\uparrow\rangle), \quad |-\rangle = |\downarrow\downarrow\rangle. \quad (2.30)$$

To understand the formalism and structure of MPS, the introduction of a mapping will lead to a simple non-trivial tensor network as a solution for the ground state.

The ground state of the Hamiltonian in Eq. 2.24 according to Eq. 2.29 should consist of links which *never* yield a total spin-2 state. Such a state can be obtained by a spin-1 chain with two symmetrised spin-1/2 subcomponents projected onto a triplet state at each lattice point. All neighbouring spin-1/2 pairs of adjacent spin-1 systems contract to a singlet state with spin-0.

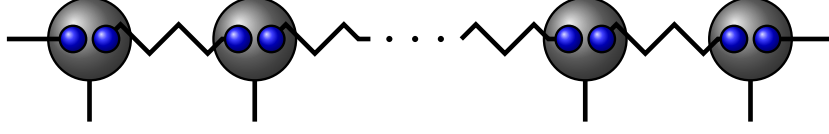


Figure 5: AKLT state for OBC. The grey tensors with a leg at the bottom represents a contraction of the two (blue) virtual spin-1/2 to a physical spin-1. The zigzag line is a symbol for singlet bounds between neighbouring spin-1/2. By construction, the border spin-1/2 are free.

For PBC, this ground state is unique with singlets for each neighbouring spin-1/2 pair. The OBC ground state has a four-fold degeneracy given by the two unbounded spin-1/2 at the borders, which are able to form a singlet and the so called *Kennedy triplet*.

Let $|\mathbf{a}\rangle = |a_1 \dots a_L\rangle$, $|\mathbf{b}\rangle = |b_1 \dots b_L\rangle$ be the representation of the left and right spin-1/2 on each point. The state $|\psi\rangle$ can be written in terms of its subcomponents

$$|\psi\rangle = \sum_{\mathbf{a}} \sum_{\mathbf{b}} c_{\mathbf{ab}} |\mathbf{ab}\rangle . \quad (2.31)$$

One may consider the bonding condition

$$|\Sigma^{[i]}\rangle = \sum_{b_i a_{i+1}} \Sigma_{b_i a_{i+1}} |b_i a_{i+1}\rangle \quad (2.32)$$

and rewrite the four constants $\Sigma_{b_i a_{i+1}}$ as a 2×2 matrix

$$\Sigma = \begin{pmatrix} 0 & \frac{1}{\sqrt{2}} \\ -\frac{1}{\sqrt{2}} & 0 \end{pmatrix} . \quad (2.33)$$

One is now able to write the total state with singlet-bonded spin-1/2 particles

$$|\psi_{\Sigma}\rangle = \sum_{\mathbf{a}} \sum_{\mathbf{b}} \Sigma_{b_1 a_2} \Sigma_{b_2 a_3} \dots \Sigma_{b_{L-1} a_L} |\mathbf{ab}\rangle . \quad (2.34)$$

The state is given by a product of matrices, where the local states are composed of its two constituents. To include the projection to physical spin-1, one has to define a mapping operator M_{ab}^{σ} , which acts on $|\sigma\rangle \langle ab|$. In matrix form, this yields

$$M^+ = \begin{pmatrix} 1 & 0 \\ 0 & 0 \end{pmatrix} , \quad M^0 = \begin{pmatrix} 0 & \frac{1}{\sqrt{2}} \\ \frac{1}{\sqrt{2}} & 0 \end{pmatrix} , \quad M^- = \begin{pmatrix} 0 & 0 \\ 0 & 1 \end{pmatrix} . \quad (2.35)$$

Therefore the total state can be expressed by

$$|\psi\rangle = \sum_{\sigma} \sum_{\mathbf{a}, \mathbf{b}} M_{a_1 b_1}^{\sigma_1} \Sigma_{b_1 a_2} M_{a_2 b_2}^{\sigma_2} \Sigma_{b_2 a_3} \dots \Sigma_{b_{L-1} a_L} M_{a_L b_L}^{\sigma_L} |\sigma\rangle , \quad (2.36)$$

or equivalently by the AKLT matrices $A^{\sigma} \propto M^{\sigma} \Sigma$, normalised in the thermodynamic limit (system size $L \rightarrow \infty$)

$$A^+ = \begin{pmatrix} 0 & \sqrt{\frac{2}{3}} \\ 0 & 0 \end{pmatrix} , \quad A^0 = \begin{pmatrix} -\sqrt{\frac{1}{3}} & 0 \\ 0 & \sqrt{\frac{1}{3}} \end{pmatrix} , \quad A^- = \begin{pmatrix} 0 & 0 \\ -\sqrt{\frac{2}{3}} & 0 \end{pmatrix} . \quad (2.37)$$

The explicit form of a wave function

$$|\psi\rangle = \sum_{\sigma_1 \dots \sigma_L} A_{\sigma_1}^{[1]} A_{\sigma_2}^{[2]} \dots A_{\sigma_{L-1}}^{[L-1]} A_{\sigma_L}^{[L]} |\sigma_1 \sigma_2 \dots \sigma_{L-1} \sigma_L\rangle, \quad (2.38)$$

with rank-3 tensors $A^{[i]}$ of - in general - site-dependent dimensions ($m_i \times m_{i+1} \times d_i$) is called a 1D *matrix product state* (MPS). For the AKLT model, the matrices $A_{\sigma_i}^{[i]}$ are, except for the borders, all equal and of dimension $((m_i = 2) \times (m_{i+1} = 2) \times (d_i = 3))$. Hence the total expression becomes simpler. To conclude in a short summary: One is able to rewrite the ground state as a MPS by introduction of maximally entangled subcomponents. Moreover, the auxiliary dimensions of the tensors are constant, even though the Hilbert space grows exponentially with the system size.

Sequential Singular Value Decomposition

In fact, the MPS structure of Eq. 2.38 can be obtained for any arbitrary spin-1 state

$$|\psi\rangle = \sum_{\sigma_1 \dots \sigma_L} c_{\sigma_1 \dots \sigma_L} |\sigma_1 \dots \sigma_L\rangle, \quad (2.39)$$

with 3^L coefficients $c_{\sigma_1 \dots \sigma_L}$ via sequential singular value decomposition (SSVD). The main idea is represented graphically in Fig. 6 and consists of the following steps:

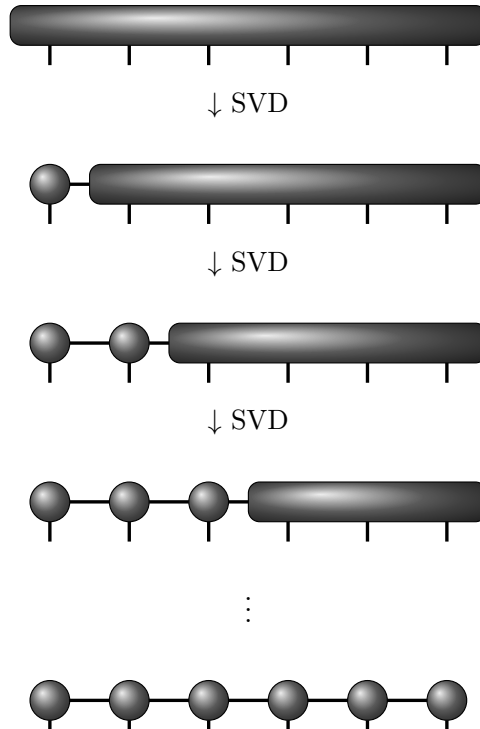


Figure 6: Starting from $\Psi_{\sigma_1, \dots, \sigma_L}$ the MPS can be gained via sequential reshaping, SVD and permutation - if needed.

1. Write the 3^L coefficients $c_{\sigma_1, \dots, \sigma_L}$ in a tensor $\Psi_{\sigma_1 \dots \sigma_L}$ of dimensions $\underbrace{(3 \times 3 \cdots \times 3 \times 3)}_L$.
2. Reshape the tensor as a matrix $\Psi_{\sigma_1 \dots \sigma_L} \rightarrow \tilde{\Psi}_{\sigma_1(\sigma_2 \dots \sigma_L)}$.
3. A SVD of $\tilde{\Psi}_{\sigma_1(\sigma_2 \dots \sigma_L)}$ yields

$$\tilde{\Psi}_{\sigma_1(\sigma_2 \dots \sigma_L)} = \sum_{\alpha_1=1}^{r_1} U_{\sigma_1 \alpha_1} \Lambda_{\alpha_1 \alpha_1} V_{\alpha_1(\sigma_2 \dots \sigma_L)}^\dagger. \quad (2.40)$$

4. Reshape $U_{\sigma_1 \alpha_1}$ into a tensor $U_{\alpha_1}^{\sigma_1} \equiv \Gamma_{\alpha_1}^{\sigma_1}$, reshape the matrix $\Lambda_{\alpha_1 \alpha_1} V_{\alpha_1(\sigma_2 \dots \sigma_L)}^\dagger \rightarrow \tilde{V}_{(\alpha_1 \sigma_2)(\sigma_3 \dots \sigma_L)}$ and make another SVD to obtain

$$V_{(\alpha_1 \sigma_2)(\sigma_3 \dots \sigma_L)} = U_{(\alpha_1 \sigma_2) \alpha_2} \Lambda_{\alpha_2 \alpha_2} V_{\alpha_2(\sigma_3 \dots \sigma_L)}^\dagger. \quad (2.41)$$

5. Reshape $U_{(\alpha_l \sigma_{l+1}) \alpha_{l+1}} \rightarrow \Gamma_{\alpha_l \alpha_{l+1}}^{\sigma_{l+1}}$ and repeat the SVD with $\Lambda_{\alpha_{l+1} \alpha_{l+1}} V_{\alpha_{l+1}(\sigma_{l+2} \dots \sigma_L)}^\dagger$ for $l = 1 \dots (L-2)$.
6. Reshape the matrix $\Lambda_{\alpha_{L-1} \alpha_{L-1}} V_{\alpha_{L-1} \sigma_L}^\dagger \rightarrow \Gamma_{\alpha_{L-1}}^{\sigma_L}$.

Note

Of course, at each step, the matrices U , Λ , V and Γ are different. Therefore, the coefficients $c_{\sigma_1 \dots \sigma_L}$ are given by the contraction of L different Γ matrices

$$c_{\sigma_1 \dots \sigma_L} = \Gamma_{\sigma_1}^{[1]} \Gamma_{\sigma_2}^{[2]} \dots \Gamma_{\sigma_{L-1}}^{[L-1]} \Gamma_{\sigma_L}^{[L]}. \quad (2.42)$$

A naive decomposition would yield a splitting into matrices with exponential increasing dimensions. However, the SVD reveals that these dimensions can be significantly decreased due to the fact that information between two subsystems is limited. In the case of the AKLT state, the Schmidt rank is even constant: $m = 2$. This agrees with the construction of the exact solution we illustrated before, despite the matrices obtained by SSVD are in general quite different from the A 's of Eq. 2.38. This has to do with the so called *gauge freedom* of the tensors, a property that we will explain and exploit later on to get convenient MPS forms (see chapter 2.6).

2.5 MATRIX PRODUCT OPERATORS

Given a physical state in MPS form according to Eq. 2.42

$$\langle \boldsymbol{\sigma} | \psi \rangle = \Gamma_{\sigma_1}^{[1]} \Gamma_{\sigma_2}^{[2]} \dots \Gamma_{\sigma_{L-1}}^{[L-1]} \Gamma_{\sigma_L}^{[L]}, \quad (2.43)$$

in order to calculate expectation values, it is numerically profitable to work with an analogue representation for operators O

$$\langle \boldsymbol{\sigma} | O | \boldsymbol{\sigma}' \rangle = \Omega_{\sigma_1 \sigma'_1}^{[1]} \Omega_{\sigma_2 \sigma'_2}^{[2]} \dots \Omega_{\sigma_{L-1} \sigma'_{L-1}}^{[L-1]} \Omega_{\sigma_L \sigma'_L}^{[L]}. \quad (2.44)$$

This is possible for any operator, because it can be written such that

$$O = \sum_{\sigma_1 \dots \sigma_L} \sum_{\sigma'_1 \dots \sigma'_L} c_{(\sigma_1 \dots \sigma_L)(\sigma'_1 \dots \sigma'_L)} |\sigma\rangle \langle \sigma'|, \quad (2.45)$$

and therefore be decomposed analogue to Fig. 6 via SSVD, but with two physical indices σ_i, σ'_i instead of only one. This means for the graphical notation, each tensor of a matrix product operator (MPO) at site j is of rank-4 and the pictorial representation is with two vertical lines - one for an ingoing quantum number and one for an outgoing one. The final MPO then has two physical legs in vertical direction and two auxiliary legs in horizontal direction (see Fig. 7). The border tensors can be written with dummy indices, too.

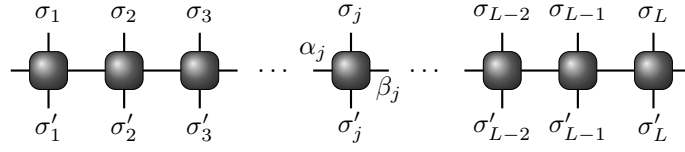


Figure 7: MPO chain with L sites. Each tensor $\Omega_{\alpha_j \beta_j}^{\sigma_j \sigma'_j}$ at site j has two physical indices σ_j, σ'_j and two auxiliary indices α_j, β_j .

Fortunately, for an operator expressed as sums of local operators (e.g. link model Hamiltonian or magnetisation), it is possible to directly write down the MPO form. To do so, reconsider the local block $\Omega^{\sigma\sigma'}$ with its projector $|\sigma\rangle \langle \sigma'|$ to obtain a local operator $\hat{\Omega}^i = \sum_{\sigma\sigma'} \Omega^{\sigma\sigma'} |\sigma\rangle \langle \sigma'|$ acting on the local quantum numbers σ and σ' . The total operator becomes a composition of operators acting on different local Hilbert spaces

$$O = \hat{\Omega}^1 \hat{\Omega}^2 \dots \hat{\Omega}^L. \quad (2.46)$$

Hence, contractions of such operator-valued tensors results in a sum of tensor products of their corresponding operators. A simple example should explain the basic principle of the form for the compact Hamiltonian. The 1D Ising Hamiltonian in a transverse field with OBC is given by

$$H_{\text{Ising}} = - \sum_{i=1, j=1}^L J_{ij} S_i^x S_j^x - \Gamma \sum_{i=1}^L S_i^z. \quad (2.47)$$

$S^{x/z} = \frac{1}{2} \sigma_{x/z}$ are spin operators (in this thesis, $\hbar = c_0 = 1$ for simplicity). In the following, we assume this coupling to be constant for each particle pair: $J_{ij} = 0$ for $j \neq i + 1$, and $J_{i, i+1} = \text{const.} = J$. Explicitly, the Hamiltonian takes the form

$$\begin{aligned} H &= -JS_x \otimes S_x \otimes \mathbb{1} \otimes \mathbb{1} \otimes \dots \otimes \mathbb{1} - hS_z \otimes \mathbb{1} \otimes \mathbb{1} \otimes \dots \otimes \mathbb{1} \\ &\quad - \mathbb{1} \otimes JS_x \otimes S_x \otimes \mathbb{1} \otimes \dots \otimes \mathbb{1} - \mathbb{1} \otimes hS_z \otimes \mathbb{1} \otimes \dots \otimes \mathbb{1} \\ &\quad \dots \\ &\quad - \mathbb{1} \otimes \mathbb{1} \otimes \dots \otimes \mathbb{1} \otimes JS_x \otimes S_x - \mathbb{1} \otimes \mathbb{1} \otimes \dots \otimes hS_z \otimes \mathbb{1} \\ &\quad - \mathbb{1} \otimes \mathbb{1} \otimes \dots \otimes \mathbb{1} \otimes hS_z. \end{aligned} \quad (2.48)$$

This Hamiltonian can be efficiently described using the tensors in Fig. 8, where the assignment of the matrices to the vertical legs only allows for combinations appearing in the above Hamiltonian.

Figure 8: Local tensors of the Ising model in MPO representation. Note that only terms that appear in the sum can also appear in the final contraction due to the "else = 0" condition.

After a contraction of two local Hamiltonian tensors $\Omega_{\alpha\beta}^{\sigma_i\sigma'_i\sigma_j\sigma'_j} = \sum_{\gamma} \Omega_{\alpha\gamma}^{\sigma_i\sigma'_i} \Omega_{\gamma\beta}^{\sigma_j\sigma'_j}$, multiplications that do not occur in the sum are forbidden by the last condition in Fig. 8. In addition, except of an increase in matrix size, they leave the MPS form invariant:

$$\begin{aligned}
 O|\psi\rangle &= \sum_{a,b,\sigma,\sigma'} \Omega_{1,b_1}^{\sigma_1\sigma'_1} \Omega_{b_1,b_2}^{\sigma_2\sigma'_2} \dots \Omega_{b_{L-1},b_L}^{\sigma_{L-1}\sigma'_{L-1}} \Omega_{b_L,1}^{\sigma_L\sigma'_L} \Gamma_{1,a_1}^{\sigma'_1} \Gamma_{a_1,a_2}^{\sigma'_2} \dots \Gamma_{a_{L-1},a_L}^{\sigma'_{L-1}} \Gamma_{a_L,1}^{\sigma'_L} |\sigma\rangle \\
 &= \sum_{a,b,\sigma,\sigma'} \left(\Omega_{1,b_1}^{\sigma_1\sigma'_1} \Gamma_{1,a_1}^{\sigma'_1} \right) \left(\Omega_{b_1,b_2}^{\sigma_2\sigma'_2} \Gamma_{a_1,a_2}^{\sigma'_2} \right) \dots \left(\Omega_{b_{L-1},b_L}^{\sigma_{L-1}\sigma'_{L-1}} \Gamma_{a_{L-1},a_L}^{\sigma'_{L-1}} \right) \left(\Omega_{b_L,1}^{\sigma_L\sigma'_L} \Gamma_{a_L,1}^{\sigma'_L} \right) |\sigma\rangle \\
 &= \sum_{\sigma} N_{\sigma_1}^{[1]} N_{\sigma_2}^{[2]} \dots N_{\sigma_{L-1}}^{[L-1]} N_{\sigma_L}^{[L]} |\sigma\rangle, \text{ with } N_{\sigma_j}^{[j]} = \left(N_{(b_j a_j), (b_{j+1} a_{j+1})}^{[j] \sigma_j} \right).
 \end{aligned} \tag{2.49}$$

For energy calculations this form is really comfortable, because one does not need any book-keeping of different contributions to the energy but has all together in a self-similar notation.

2.6 GENERATION OF CANONICAL STATES

For open boundary conditions, it is sufficient to construct a MPS which provides orthogonality, i.e. $\langle\psi|\psi\rangle = 1$. This may be obtained by the *gauge* property of MPS. Due to the laws for matrix multiplication, one is free to add an identity between two tensors, e.g.

$$\mathbb{1} = QQ^\dagger, \tag{2.50}$$

which transforms the MPS into a different appearance. Given an arbitrary MPS

$$|\psi\rangle = \sum_{\sigma_1\sigma_2\sigma_3\dots} \sum_{a_1 a_2 a_3\dots} M_{1,a_1}^{\sigma_1} M_{a_1,a_2}^{\sigma_2} M_{a_2,a_3}^{\sigma_3} \dots |\sigma_1\sigma_2\sigma_3\dots\rangle, \tag{2.51}$$

each tensor M^{σ_i} can be transformed into $\tilde{M}^{\sigma_i} = QM^{\sigma_i}Q^\dagger$ without changing the resulting contraction, which can be easily shown.

$$\begin{aligned}
|\tilde{\psi}\rangle &= \sum_{\sigma_1\sigma_2\sigma_3\dots} \sum_{a_1a_2a_3\dots} \tilde{M}_{1,a_1}^{\sigma_1} \tilde{M}_{a_1,a_2}^{\sigma_2} \tilde{M}_{a_2,a_3}^{\sigma_3} \dots |\sigma_1\sigma_2\sigma_3\dots\rangle \\
&= \sum_{\mathbf{a}} \sum_{\mathbf{b}} \sum_{\boldsymbol{\sigma}} (M_{1,b_1}^{\sigma_1} Q_{b_1,a_1}^\dagger) (Q_{a_1,b_2} M_{b_2,b_3}^{\sigma_2} Q_{b_3,a_2}^\dagger) (Q_{a_2,b_4} M_{b_4,b_5}^{\sigma_3} Q_{b_5,a_3}^\dagger) \dots |\boldsymbol{\sigma}\rangle \\
&= \sum_{\sigma_1\sigma_2\sigma_3\dots} \sum_{a_1a_2a_3\dots} M_{1,a_1}^{\sigma_1} M_{a_1,a_2}^{\sigma_2} M_{a_2,a_3}^{\sigma_3} \dots |\sigma_1\sigma_2\sigma_3\dots\rangle \\
&= |\psi\rangle
\end{aligned} \tag{2.52}$$

This property allows to change the tensor form of states to obtain a numerically cheaper expression for optimised calculations.

For example, one can demand *left* or *right normalised states* for further calculations in order to simplify a given problem - e.g. iterative ground state search or local magnetisations, correlations and so on. This will be explained in more detail in chapter 2.7-2.9.

Left Normalised Canonical States

For a general state

$$|\psi\rangle = \sum_{\boldsymbol{\sigma}} \sum_{a_1\dots} M_{1,a_1}^{\sigma_1} M_{a_1,a_2}^{\sigma_2} M_{a_2,a_3}^{\sigma_3} \dots |\boldsymbol{\sigma}\rangle, \tag{2.53}$$

a SVD of $M_{1,a_1}^{\sigma_1} \rightarrow M_{(\sigma_1,1),a_1} = \sum_{s_1} U_{(\sigma_1,1),s_1} S_{s_1,s_1} V_{s_1,a_1}^\dagger$ yields a left normalised tensor $U_{1,s_1}^{\sigma_1}$. S and V^\dagger can be multiplied to M^{σ_2} according to

$$\begin{aligned}
|\psi\rangle &= \sum_{\boldsymbol{\sigma}} \sum_{a_1,a_2,\dots} \sum_{s_1} U_{1,s_1}^{\sigma_1} S_{s_1,s_1} V_{s_1,a_1}^\dagger M_{a_1,a_2}^{\sigma_2} \dots |\boldsymbol{\sigma}\rangle \\
&= \sum_{\boldsymbol{\sigma}} \sum_{a_2,\dots} \sum_{s_1} U_{1,s_1}^{\sigma_1} \left(\sum_{a_1} S_{s_1,s_1} V_{s_1,a_1}^\dagger M_{a_1,a_2}^{\sigma_2} \right) M_{a_2,a_3}^{\sigma_3} \dots |\boldsymbol{\sigma}\rangle \\
&= \sum_{\boldsymbol{\sigma}} \sum_{a_2,\dots} \sum_{s_1} U_{1,s_1}^{\sigma_1} \tilde{M}_{s_1,a_2}^{\sigma_2} M_{a_2,a_3}^{\sigma_3} \dots |\boldsymbol{\sigma}\rangle.
\end{aligned} \tag{2.54}$$

If one is not interested explicitly in singular values of M^{σ_i} , QR decomposition (QRD) is more effective and yields the same effect of canonisation (see attachment, section B.2). A sequential decomposition following the previous scheme leads to a set of left normalised tensors for the MPS. The last decomposition of $\tilde{M}_{a_{L-1},1}^{\sigma_L}$ contains the scalar $S_{1,1} V_{1,1}^\dagger$, which is the norm of $|\psi\rangle$ and can be set to 1.

Right Normalised Canonical States

The procedure is analogue, but the reshaping is $M_{a_{i-1},a_i}^{\sigma_i} \rightarrow M_{a_{i-1},(a_i\sigma_i)}$ and the process direction is inverted

$$\begin{aligned}
 |\psi\rangle &= \sum_{\sigma} \sum_{a_{L-1}, \dots} \dots M_{a_{L-2}, a_{L-1}}^{\sigma_{L-1}} M_{a_{L-1}, 1}^{\sigma_L} |\sigma\rangle \\
 &= \sum_{\sigma} \sum_{a_{L-2}, \dots, s_{L-1}} \dots M_{a_{L-2}, a_{L-1}}^{\sigma_{L-1}} \left(U_{a_{L-1}, s_{L-1}} S_{s_{L-1}, s_{L-1}} V_{s_{L-1}, 1}^{+\sigma_L} \right) |\sigma\rangle \\
 &= \sum_{\sigma} \sum_{a_{L-2}, \dots, s_{L-1}} \dots M_{a_{L-3}, a_{L-2}}^{\sigma_{L-2}} \tilde{M}_{a_{L-2}, s_{L-1}}^{\sigma_{L-1}} V_{s_{L-1}, 1}^{+\sigma_L} |\sigma\rangle .
 \end{aligned} \tag{2.55}$$

A nice feature working with this basis is that the general eigenvalue problem introduced in the next chapter becomes simpler, because the norm of a MPS with two open indices becomes the identity - represented by a black line in graphical notation.

Note

Left or right normalised canonical representation can only be approached for OBC. This is easy to see, because for PBC the contraction of site L and site 1 the normalisation has to fulfill left *and* right self-orthogonality. For now, let us not consider this and continue with left *or* right canonical MPS.

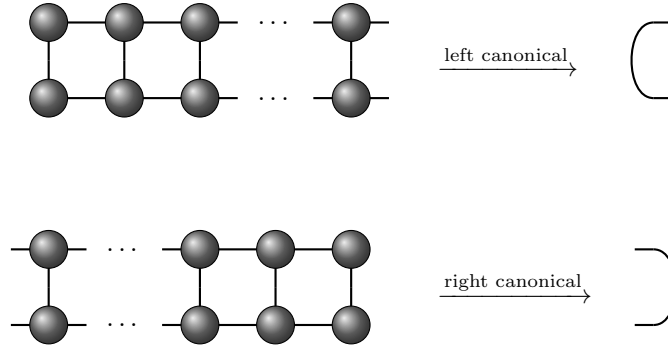


Figure 9: Canonical gauges yield a very useful normalisation of the MPS, as they allow to avoid the contraction of the responding sides during the calculation.

2.7 ITERATIVE SEARCH FOR GROUND STATES

The main idea of this chapter is to find a MPS representation for the ground state (with energy E_0). Consider the MPS with the same bond dimensions at state j : m_j, m_{j+1} , and physical dimension d . This belongs to a set of MPS

$$\mathcal{F} = \left\{ |\psi\rangle = \prod_{j=1}^L M_{\sigma_j}^{[j]} \otimes_{i=1}^L |\sigma_i\rangle \mid M^{[j]} \text{ is a } (m_j \times m_{j+1} \times d) \text{ tensor} \right\} . \tag{2.56}$$

One tries to implement an algorithm, which finds the state $|\psi'\rangle$ that minimises the energy

$$\frac{\langle \psi' | H | \psi' \rangle}{\langle \psi' | \psi' \rangle} = \min_{|\psi\rangle \in \mathcal{F}} \frac{\langle \psi | H | \psi \rangle}{\langle \psi | \psi \rangle} = E_0 . \quad (2.57)$$

This expression is equivalent to the eigenvalue problem $H|\psi\rangle = \lambda N|\psi\rangle$, which is represented by the pictorial notation in Fig. 10.

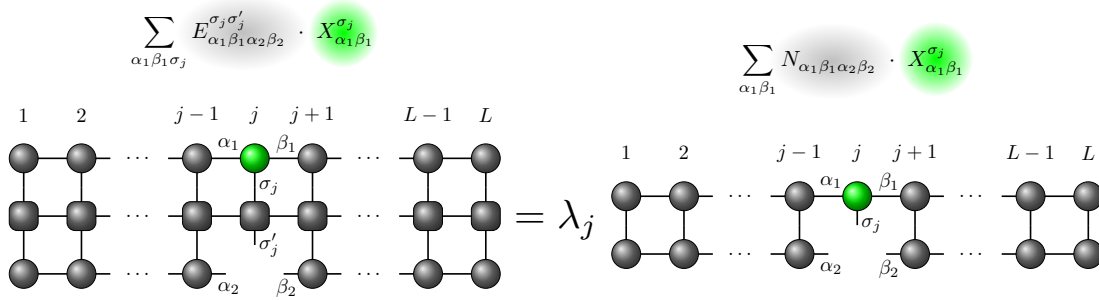


Figure 10: It is convenient to write the contraction with the searched local vector at site j (green tensor) as an operator $E^{\sigma_j \sigma'_j}$ (the contraction of all grey tensors at the left side), which acts on an arbitrary tensor $Y^{\sigma_j}_{\alpha_1 \beta_1}$ like a vector transformation $E^{\sigma_j \sigma'_j}_{\alpha_1 \beta_1 \alpha_2 \beta_2} Y^{\sigma_j}_{\alpha_1 \beta_1} = Y^{\sigma'_j}_{\alpha_2 \beta_2}$. Due to the normalisation condition $NY^{\sigma_j} = Y^{\sigma_j}$ (see Fig. 11), the canonical form simplifies the resulting generalised eigenvalue problem to a common eigenvalue problem $E^{\sigma_j \sigma'_j} X^{\sigma_j} = \lambda_j NX^{\sigma_j} = \lambda_j X^{\sigma_j}$.

To reduce calculation effort, it is reasonable to use the Hamiltonian in MPO representation (see chapter 2.5) and the MPS in canonical form. Thereby the problem can be simplified to $H|\psi\rangle = \lambda|\psi\rangle$, as left and right normalisation yield a normed state. One has to build the contraction of MPS and MPO according to Fig. 10. The effective Hamiltonian $E^{\sigma_j \sigma'_j}_{\alpha_1 \beta_1 \alpha_2 \beta_2}$ (the contraction of all grey tensors at the left side of Fig. 10) has to consist of three subparts:

1. A contraction of a left canonical MPS, its complex conjugate and all local MPO sandwiched between them from site 1 to $j-1$,
2. An additional Hamiltonian MPO at site j ,
3. A similar object as 1., but right canonical from site L to site $j+1$.

A detailed instruction for the left subpart of the effective Hamiltonian is provided in the next chapter. For now, it is more useful to understand what to do with this object. The effective Hamiltonian is hermitian by construction and all eigenvalues are real and refer directly to the state's energy. Also, in order to obtain a left or right normalised canonical MPS, a total SVD is not needed, because after each optimisation step one is just interested in the correct normalisation, which can be provided from the faster QRD. This conserves the property for the norm of the MPS, $\langle \psi_{1\dots j-1}^{\alpha_2} | \psi_{1\dots j-1}^{\alpha_1} \rangle = \delta_{\alpha_2 \alpha_1}$ and $\langle \psi_{j+1\dots L}^{\beta_2} | \psi_{j+1\dots L}^{\beta_1} \rangle = \delta_{\beta_2 \beta_1}$. To obtain a MPS with optimally approximated energy,

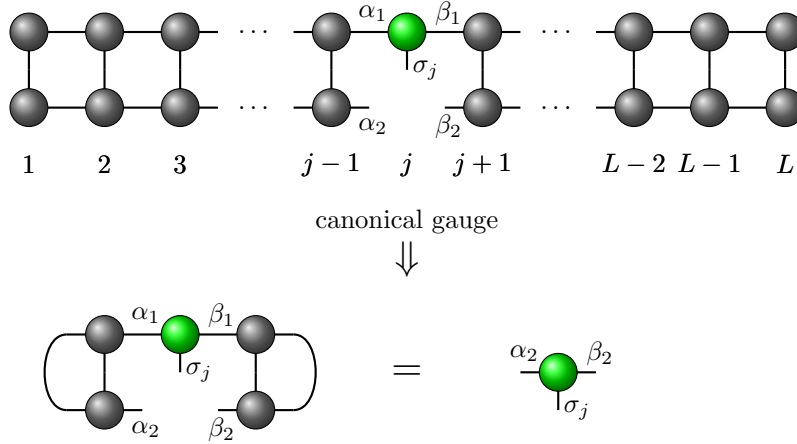


Figure 11: If the MPS becomes gauged after each iteration step, the generalised eigenvalue problem becomes a common one which yields better numerical stability.

one has to find the eigenvalues and eigenvectors for the effective Hamiltonian for each lattice position j . After finding the best local tensor to a corresponding minimal eigenvalue, the effective Hamiltonian has to be constructed with this tensor at its correct position and the next lattice point has to be optimised. One has to be careful about norming the tensor, because it depends on the direction of the routine: If the direction is from $L \rightarrow 1$, the tensor has to be right canonical and otherwise left canonical. When this procedure in one direction is completed, i.e. the last position is optimised and gauged, the direction is inverted and the routine continues. One finished left and right optimisation over the whole chain is called *sweep*. The procedure is finished, if the specified number of sweeps or accuracy is reached. Since the bond dimension m denotes the amount of considered singular values, which corresponds directly to the amount of Schmidt coefficients, this approach truncates entanglement.

This method of finding the ground states is the essence of DMRG algorithms, first proposed by Stephen R. White in 1993. A detailed introduction of the slightly different variational principle can be found in his paper from 1993 [20]. It is based on Wilson's numerical renormalisation group method⁴ [22]. Whereas Wilson used an energetic argument, White cut away states which correspond to a low probability, given by the eigenvalues of the reduced density matrix. This matrix is obtained from a successively two-site growing system in contrast to the provided routine here. The variational MPS approach is equivalent to the non-classical single-site DMRG.

⁴ The exact diagonalisation of a Hamiltonian in recursive relation form for a successively growing chain is done until the specified accuracy is reached. The numerical difficulty is to diagonalise exactly for an exponentially increasing number of states, therefore only the eigenstates of the lowest many particle energies are kept. In this way, the dimension of the Hamiltonian is fixed and the computation time increases linearly with the total chain length [2].

2.8 BUILDING THE EFFECTIVE HAMILTONIAN

This section gives the idea of the contraction steps for the effective Hamiltonian $E^{\sigma_j \sigma'_j}$. The fundamental basis of the construction effort is given by the a-priori tensor structure of MatLab arrays. Therefore, a contraction of two tensors is performed by reshaping, matrix multiplication and a final reshaping to the needed tensor form - also index permutations, if needed. For now, the steps for the left side of the effective Hamiltonian will be provided, the right side can be constructed in a similar way. In the following, ${}^i_L H$ will be the resulting tensor of a contraction from site $1 \rightarrow i$ of the left canonical MPS with its complex conjugate and a MPO sandwiched between each site, according to the left portion of the effective Hamiltonian in Fig. 10. A special case may be the border locations, but we will introduce a left initial tensor ${}^0_L H_{\alpha\beta\gamma}$ in order to make every contraction equal.

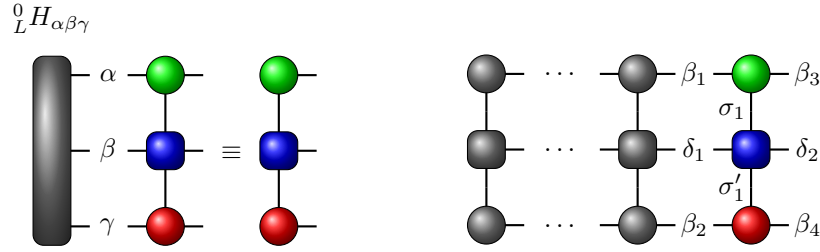


Figure 12: Contraction steps for the left side of the effective Hamiltonian $E^{\sigma_j \sigma'_j}$. Assume that one contracts the grey tensor (which contains the contraction of i left-canonical sites and the corresponding Hamiltonians in MPO form) ${}^i_L H_{\beta_1 \delta_1 \beta_2}$ with the coloured tensors.

For simplicity and reasons of book-keeping, it is important to maintain a consistent way of labelling the legs of the various tensors. In the following, the labelling is from left side - top to bottom, to right side - top to bottom. Given a tensor of the MPS $A_{\alpha_1 \beta_1}^{\sigma_1}$ of physical dimension d and bond dimensions m . The Hamiltonian in MPO form has the same physical dimension d and the auxiliary dimension is assumed⁵ to be n . In order to process a sequential contraction, it is highly recommended to draw the situation before implementing it. The first step - away from the border $i > 0$ - is a multiplication of

$${}^i_L \tilde{H}_{(\delta_1 \beta_2)(\beta_3 \sigma_1)} = \sum_{\beta_1} {}^i_L H_{(\delta_1 \beta_2) \beta_1} A_{\beta_1 (\beta_3 \sigma_1)}. \quad (2.58)$$

A reshape to the correct index dimensions and permutation leads to the temporary object ${}^i_L H_{\beta_3 \sigma_1 \delta_1 \beta_2}$ with the green tensor contracted. The blue local MPO $H_{\delta_1 \delta_2}^{\sigma_1 \sigma'_1} \rightarrow H'_{(\sigma_1 \delta_1)(\delta_2 \sigma'_1)}$ is combined to this expression via

$${}^i_L \tilde{H}_{(\beta_3 \beta_2)(\delta_2 \sigma'_1)} = \sum_{(\sigma_1 \delta_1)} {}^i_L \tilde{H}_{(\beta_3 \beta_2)(\sigma_1 \delta_1)} H'_{(\sigma_1 \delta_1)(\delta_2 \sigma'_1)}. \quad (2.59)$$

⁵ The auxiliary dimensions depend on the number of terms of a local Hamiltonian - e.g. 1D Ising with transverse field gives an overall $n = 3$ (except for the borders).

The last step contracts the red tensor and yields the final object

$${}_{L}^{i+1}\tilde{H}_{(\beta_3\delta_2)\beta_4} = \sum_{\sigma_1\beta_2}^{d\cdot m} {}_{L}^i\tilde{H}_{(\beta_3\delta_2)(\sigma_1\beta_2)} A_{(\sigma_1\beta_2)\beta_4}^* , \quad (2.60)$$

which may reshaped to ${}_{L}^{i+1}H_{\beta_3\delta_2\beta_4}$. For the explicit contraction of the border object ${}_{L}^0H$ with the green, blue and red tensor, the final tensor fulfills the condition $\delta_{\alpha,1}\delta_{\beta,1}\delta_{\gamma,1}$, hence ${}_{L}^0H$ has to be a $(m \times n \times m)$ tensor with a single nonzero entry ${}_{L}^0H_{1,1,1} = 1$. One may define a function $H_{\text{step}}^L(A^{[i+1]}, {}_{L}^iH)$, which builds the resulting tensor ${}_{L}^{i+1}H$ out of $A^{[i+1]}$ and ${}_{L}^iH$ according to the mentioned three contraction steps. This then provides a sufficient way to build up the left part of the effective Hamiltonian successively without a special case for the border.

The same things as mentioned can be done to build the right side of the effective Hamiltonian composed of a right canonical MPS.

In order to solve the eigenvalue problem via the MatLab function `eigs()`, it is sufficient to write a function

$$H_{\text{eff}} \left({}_{R}^jH, {}_{L}^jH, j, Y \right) , \quad (2.61)$$

which contracts the effective Hamiltonian with an arbitrary vector $Y_{(\alpha_1\beta_1\sigma_j)}$ of dimensions $(1 \times m^2d)$ and reshapes the new object $\tilde{Y}_{\alpha_2\beta_2}^{\sigma_j}$ to a $(1 \times m^2d)$ vector. With this implementation, one is able to give the function handle to `eigs`, such that

$$\begin{aligned} &\text{options.isreal} = 0; \\ &[\Lambda_j, \lambda_j] = \text{eigs} \left(@ (Y) H_{\text{eff}} \left({}_{R}^jH, {}_{L}^jH, j, Y \right), m^2d, 1, 'sr', \text{options} \right) \end{aligned} \quad (2.62)$$

solves for the eigenvector Λ_j of dimension $(1 \times m^2d)$ " m^2d " with the first "1" smallest real "sr" eigenvalue λ_j . A finished sweep is now the optimisation and left canonisation of each position $j = 1 \dots L$ and then backwards from $j = L \dots 1$. In order to obtain a simplified eigenvalue problem for each site j , after an optimisation, the resulting local state has to become gauged. Whether right or left canonical depends strictly on the current direction.

Note

For an estimation of the convergence quality, it is useful to save the eigenvalues after each computation step. Note that these eigenvalues have to fulfill the condition $\lambda_{i+1} < \lambda_i$ for every optimisation step i . After several sweeps, these values may randomly oscillate within the order of numerical precision - i.e. machine precision + error - and the optimisation may be stopped. This oscillation can be seen in the demonstration chapter in Fig. 17.

About Bond Dimensions

If the bond dimensions become large, the optimisation routine becomes very expensive, due to the total computation time for all contractions, which scales polynomially in m and d . Therefore one has to define the auxiliary dimensions not higher than necessary. The bond dimension m_j for site j cannot exceed⁶ the product $m_j \leq d \cdot \min(m_{j-1}, m_{j+1})$. This yields a "triangular" growth structure of the auxiliary dimensions $m_j \leq \min(d^j, d^{L-j})$. For the algorithm to be efficient, one truncates this growth with an upper limit and gets a trapezoidal structure of the bond dimensions. An alternative approach to this statically fixed bond dimensions can be a threshold on the singular values to be considered or cut off "on the sweep". For models like the well-known AKLT, this would lead to an upper limit $m_{\max} = 2$ without loss of information.

2.9 ENTANGLEMENT ENTROPY, CORRELATIONS AND MAGNETISATION

The global entanglement entropy between subsystems $(1 \dots l)$ and $(l + 1 \dots L)$ is simply given by a SVD of site l . It is a measure to estimate how "non-separable" the subsystems are and it summarises in a single number all kind of correlations between the subparts. The entanglement entropy for the Ising model in a transverse field can be seen in Fig. 20. Correlations $C_{i,j}$ refer to more local properties, in other words, how much site i "behaves" the same as site j , or how ordered the system looks like. The neighbour correlations of the Ising and Heisenberg model are plotted in Fig. 19 and Fig. 30. This section gives a rough overview about how to calculate such quantities using canonical states. For a given operator O , correlations $C_{i,j}$ are defined via

$$C_{i,j} = \langle O_i O_j \rangle - \langle O_i \rangle \langle O_j \rangle . \quad (2.63)$$

In literature, when talking about correlations, the second term is often not considered and only the quantity $\langle O_i O_j \rangle$ is specified.

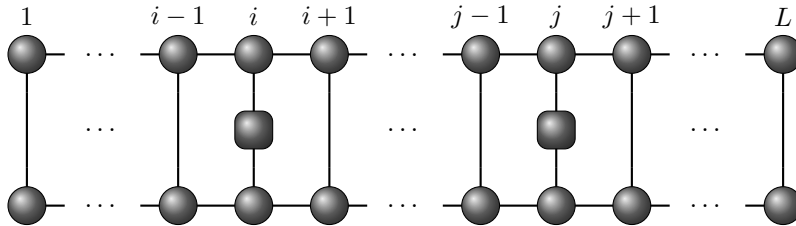


Figure 13: This contraction yields the correlations $\langle O_i, O_j \rangle$ for a given operator O of site i with site j . The black lines are representatives for the identity matrix $\mathbb{1}$. Because the MPS is gauged, the left and right side of i and j can be simplified according to figure 14.

⁶ For sure it *could* be chosen bigger, but since the rank of a matrix denotes the number of singular values, it is futile to exceed this quantity. Also note, since singular values contribute to the entanglement, the bond dimension m is a direct limit of the entanglement between each part of the MPS.

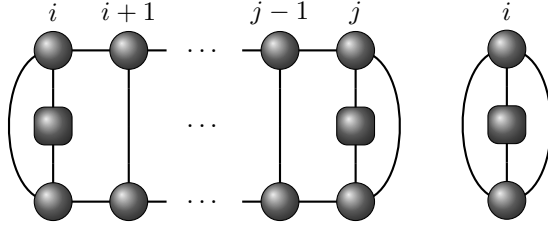


Figure 14: The contraction yields the same value for the correlation than Fig. 13 for a canonical MPS. Local quantities are obtained via the right contraction.

The correlation functions in non-gapped systems decay exponentially with the absolute distance of the sites

$$\langle O_0 O_r \rangle \propto e^{-\frac{r}{\xi}} \text{ with correlation length } \xi. \quad (2.64)$$

For ungapped systems, this relation becomes algebraic

$$\langle O_0 O_r \rangle \propto r^{-\alpha}. \quad (2.65)$$

For the purposes of this thesis, these equivalences will be taken for granted, yet a detailed derivation can be found in [10, 17]. The local quantities $\langle O_i \rangle$ can be obtained in the same manner as $\langle O_i O_j \rangle$ (see Fig. 13), but without the second sandwiched MPO between the two local tensors at site j .

APPLICATION OF MPS TO PHYSICAL MODELS

This chapter is the demonstration of the self implemented DMRG algorithm. For a comparison of numerical results, the Ising model is sufficient, because it describes a simple and integrable system. A main topic is the comparison to the analytical solution in order to demonstrate the power of DMRG algorithms. Important is here the notification of border and finite size effects, which unfortunately cannot be explained and minimised in detail. The next section is about the 1D bilinear-biquadratic spin-1 Hamiltonian, which is only integrable in a few points of the rich phase diagram. After the comparison to analytical - or published numerical - solutions, a short introduction of the entanglement spectrum provides an insight into current research topics.

3.1 THE 1D ISING MODEL IN A TRANSVERSE FIELD

The 1D Ising model with transverse field serves as a toy model for the study of phase transitions and describes well order-disorder ferroelectrics, or the magnetic ordering in materials with singlet crystal field ground state. Given L spin-1/2 particles in a row with nearest neighbour interactions, the Hamiltonian takes the form

$$H = -J \sum_{i=1}^{L-1} S_i^x S_{i+1}^x - \Gamma \sum_{i=1}^L S_i^z . \quad (3.1)$$

Γ corresponds the local transverse magnetic field and J provides the ferromagnetic short range interaction. The main purpose in variations of Γ and J is due to J providing a stable coupling between spins and therefore an order Γ destroying this order by flipping the spins. The model can be used to simulate a phase transition from ferro- ($J \gg \Gamma$) to paramagnetism ($\Gamma \gg J$). The two possible configurations in the pure ferromagnetic case $\Gamma = 0$ are

$$\begin{aligned} |\psi\rangle^\uparrow &= |\uparrow\uparrow \dots \uparrow\uparrow\rangle , \\ |\psi\rangle^\downarrow &= |\downarrow\downarrow \dots \downarrow\downarrow\rangle . \end{aligned} \quad (3.2)$$

For ferromagnetics in the cases of perturbative transverse fields $\Gamma \ll J$, there is an even and odd ground state composed of a superposition of spin-flips

$$\begin{aligned} |\psi^+\rangle &= \frac{1}{\sqrt{2}} (|\uparrow\uparrow\uparrow \dots \uparrow\rangle + |\downarrow\downarrow\downarrow \dots \downarrow\rangle) , \\ |\psi^-\rangle &= \frac{1}{\sqrt{2}} (|\uparrow\uparrow\uparrow \dots \uparrow\rangle - |\downarrow\downarrow\downarrow \dots \downarrow\rangle) , \end{aligned} \quad (3.3)$$

which yield a null net magnetisation along the x axis. Pierre Pfeuty [12] extended the solution from Lieb-Schultz-Mattis with finite-size solutions. The principal procedure

is as follows: A Jordan-Wigner transformation maps the spin Hamiltonian to fermions without spin. The spinless Hamiltonian is quadratic in Fermi annihilation and creation operators and can be diagonalised by Fourier and Bogoliubov transformations. Defining $\lambda = \frac{J}{2\Gamma}$, the resulting energy for OBC is given by [12]

$$E_0 = -\frac{\Gamma}{2} \sum_k \Lambda_k, \quad (3.4)$$

$$\Lambda_k^2 = 1 + 2\lambda \cos(k) + \lambda^2, \text{ where } k \text{ is solution of } -\lambda = \frac{\sin(k(N+1))}{\sin(kN)}.$$

There is a way to transform the Ising model into Majorana form, such that the total contribution to the ground state energy of each site is given by the overlap of boundary modes. These modes are only spanned from the Majorana operators c_1 and c_{2L} . An illustration of the resulting state is given in Fig. 15.

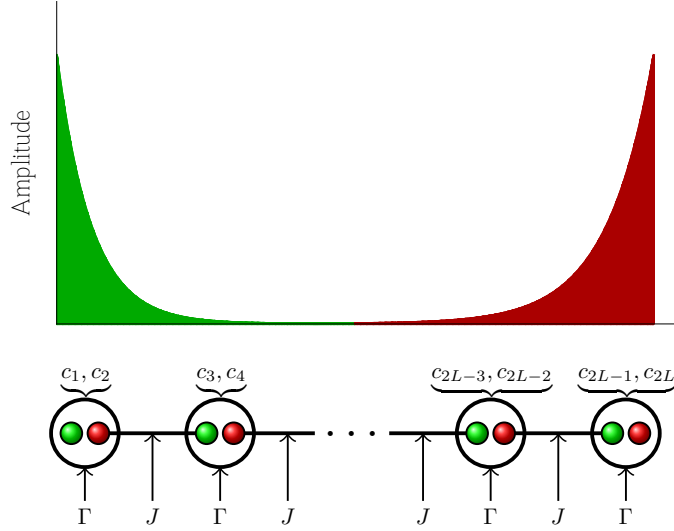


Figure 15: Pictorial representation of the Ising model Hamiltonian in Majorana form. Similarly to the AKLT state, the two border operators are unbounded. For states given by the boundary modes, contributions from each site fall off exponentially in the bulk.

We can see in the appendix C.1 that the two-fold degeneracy of the ground state is lifted by only an exponentially small splitting in system size [7], which hence is difficult to resolve numerically. This may be an explanation for slightly worse convergence or symmetry breakings for cases $\frac{2\Gamma}{J} < 1$ that can be noticed in Figs. 16, 18 and 19.

The numerical values of the analytical solution according to Eq. 3.4 for OBC have been calculated for the Ising model with transverse field. All eigenvalues have been recorded for a variation of the total number of sweeps at the pre-critical point $\Gamma = 0.5J$, in order to estimate the optimum choice between accuracy and speed for the other figures (see Fig. 17). In the ferromagnetic phase for values $2\Gamma < J$ the accuracy is slightly worse than after the critical point (see Fig. 16). This is consistent with the

quasi-degeneracy of the grounds for $\Gamma < 0.5J$, which came up in the discussion of the Ising model in Majorana form.

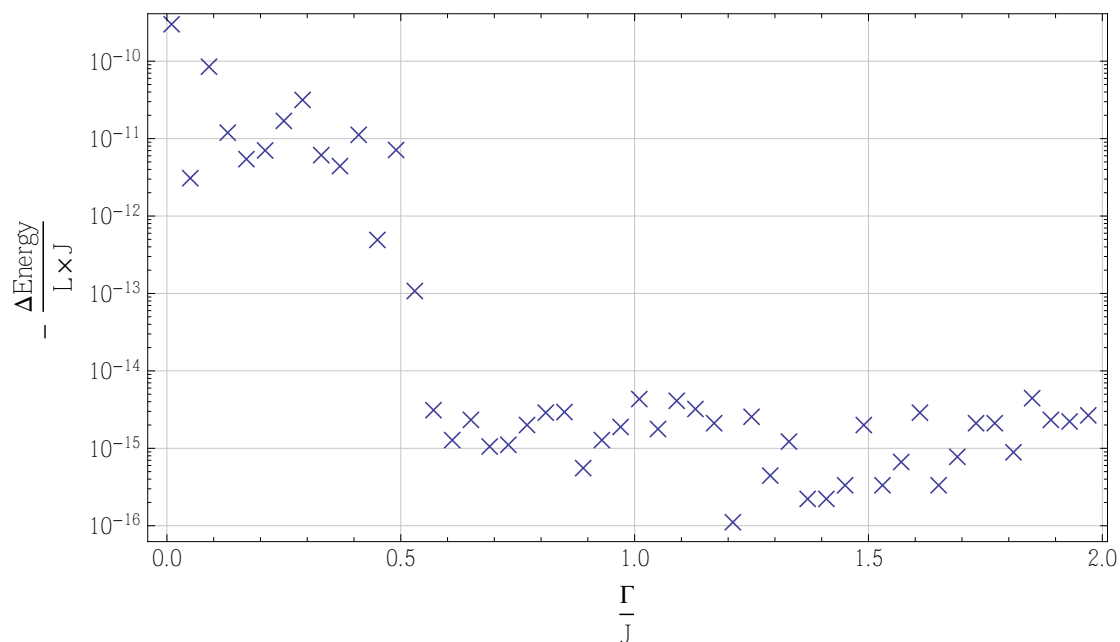


Figure 16: Absolute energy difference between numerical and analytical value in the ferromagnetic phase under change of Γ and a total number of five sweeps with $m = 50$ and $L = 100$. Especially for small transverse field constants, the DMRG converges slightly worse to the analytical solution.

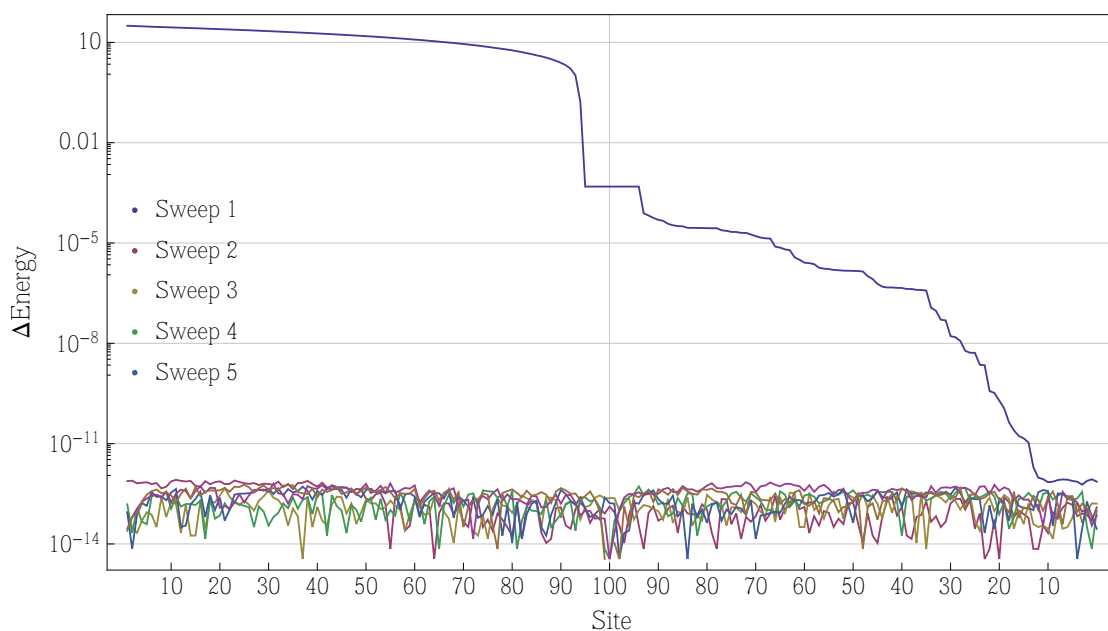


Figure 17: Absolute energy difference between numerical data and analytical solution versus sweep number at critical point of the Ising model $\frac{\Gamma}{J} = \frac{1}{2}$ with bond dimension $m = 50$ and $L = 100$ sites. If interested, in the appendix, Fig. 26 shows the convergence, when rising m .

3.1.1 Magnetisation

For the magnetisation, the Ising model ground state $|\psi^\pm\rangle$ for zero transverse field is two-fold degenerate as mentioned in Eq. 3.2 and has the magnetisation $\sum_i \langle \psi^\pm | S_i^x | \psi^\pm \rangle = \pm \frac{L}{2}$. When applying a field, the ground state is an (anti) symmetric superposition and the total magnetisation should be zero. The magnetisation graph along the z- and y-axis is as expected, whereas M_x appears to be nonzero, when a transverse field is applied to the system. This happens because any small perturbation - e.g. random tensor initialisation or start guesses for the algorithm - induces a symmetry breaking and leads to a state with nonzero global magnetisation. When m is raised, the edge where M_x drops to zero moves to the left, which gives a hint that increasing the bond dimension dims the problem, because it increases the amount of stored information between subsystems - hence, the precision in general. Again the explanation of before seems plausible, contributions of local energies decay $\epsilon_j \propto e^{-j/\xi}$ with correlation length ξ and hence the proper superposition is difficult to resolve numerically. However, the magnetisation along z-axis fits the analytical solution according to [12]

$$\begin{aligned} \langle S_i^z \rangle &= \frac{1}{2} G(0) \\ G(N) &= L(N) + \lambda L(N+1) \quad L(N) = \frac{1}{\pi} \int_0^\pi dk \Lambda_k^{-1} \cos(kN), \end{aligned} \quad (3.5)$$

with $\Lambda_k = \sqrt{1 + \lambda^2 + 2\lambda \cos(k)}$ and $\lambda = \frac{J}{2\Gamma}$ and chain length N .

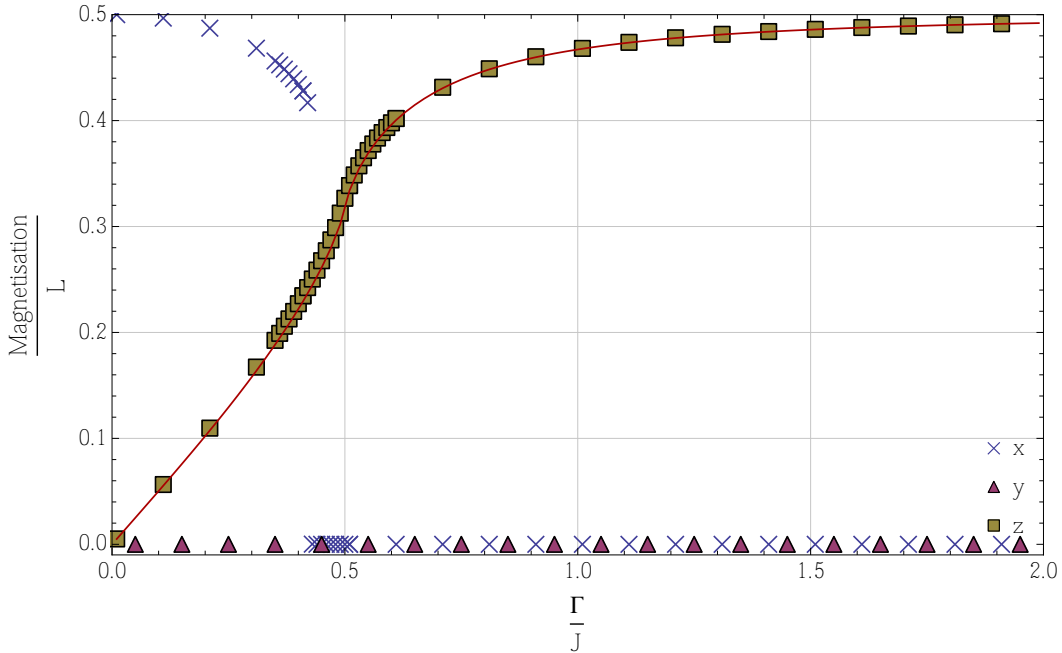


Figure 18: Absolute value $|M|$ for the magnetisation along x, y and z axis under change of Γ . $L = 100$, $m = 50$ and a total number of five sweeps. The analytical values for M_z have been calculated and are represented by the red line.

3.1.2 Correlations

The exact solutions from Pfeuty [12] provide a solution for correlators according to

$$\langle S_i^x, S_{i+1}^x \rangle = \frac{1}{4} \begin{vmatrix} G(-1) & G(-2) & \dots & G(-L) \\ G(0) & G(-1) & \dots & G(-L+1) \\ \vdots & \vdots & & \vdots \\ G(L-2) & G(L-1) & \dots & G(-1) \end{vmatrix}, \quad (3.6)$$

Fig.19 gives a comparison with numerically obtained results.

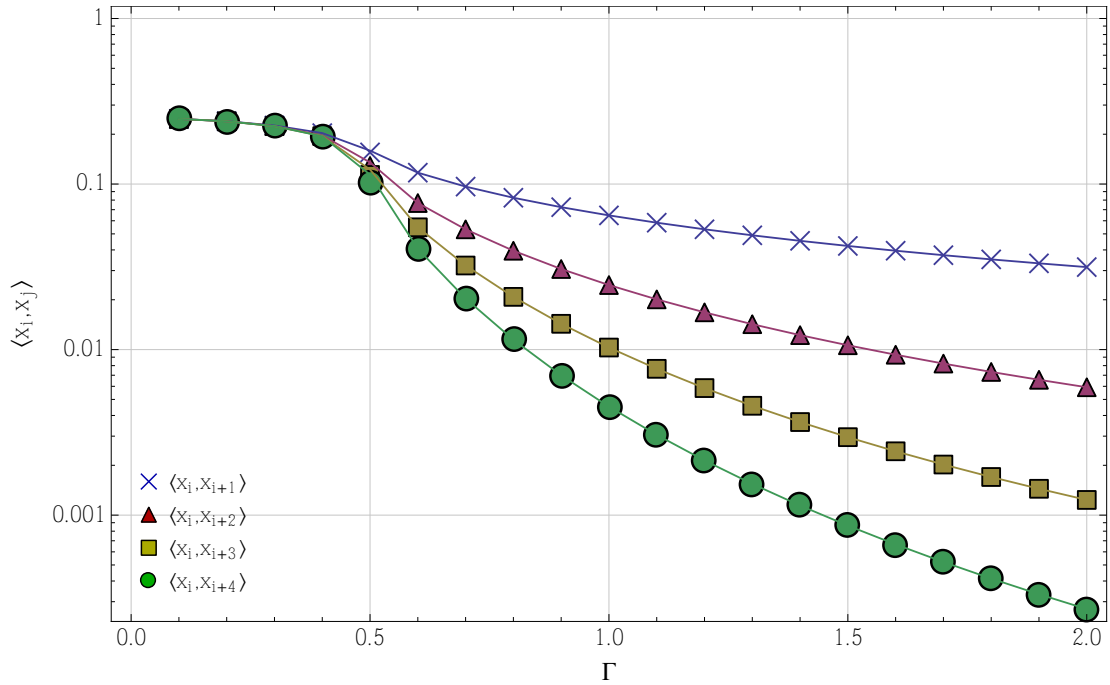


Figure 19: Neighbour correlations versus Γ . The bond dimension is $m = 25$ for a total system length of $L = 32$. The analytical solution is represented by the coloured lines, therefore the simulation quality for correlations is estimated to be very accurate.

3.1.3 Entropy

The analytical relations of the entanglement entropy are given by [19]

$$\left. \begin{aligned} S_A &= \frac{c}{3} \log_2(L) + b, \text{ for critical} \\ S_A &= \frac{c}{3} \log_2 \xi + b, \text{ for non-critical} \end{aligned} \right\} \text{field constants } \Gamma. \quad (3.7)$$

Theoretically, going to infinity for both bond dimensions and number of sites, one is able to directly read off the correlation length of the system. In this thesis, we will not

investigate further correlation lengths. Just note from Fig. 20 that the saturation point within system length is not reached when coming closer to the critical point, which is consistent with the formulation above, that the entropy obeys an area law $\propto \log(L)$.

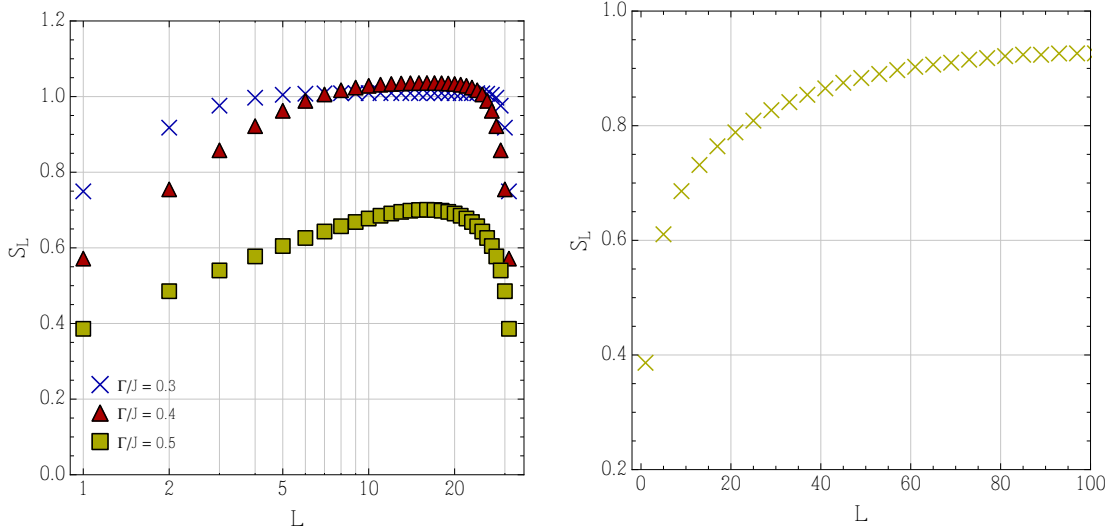


Figure 20: Plot of the entanglement entropy of the left system versus increasing subsystem size. It can be noticed quite nicely, that for non-critical transverse field the entropy gets to a saturation, whereas for critical field this saturation does not exist - at least for 32 sites. For a better notice, the right figure is a run with bond dimension $m = 100$ and $L = 200$ for the critical point $\Gamma = 0.5J$.

3.1.4 Conclusions and Perspective

It has been tried to force the DMRG to converge to one particular state $|\psi^+\rangle$, $|\psi^-\rangle$ by applying a small longitudinal field as perturbation to lift the degeneracy. But the field has found to be of order $\mathcal{O}(10^{-6})$ for $\Gamma/J = 0.1$ and $L = 100$, hence energies differ significantly from correct ones without perturbation and this method has to be considered not reasonable. Regardless of the energies' convergence to nearly machine precision, the state with zero x magnetisation for $L = 100$ sites and transverse field $\Gamma \approx 0.1$ cannot be found, even with a maximum bond dimension $m = 500^1$. This is in agreement with the discussion, that the lifting between the quasi degenerate state is most probably below machine precision for $L = 100$. Another strategy to obtain a proper superposition could be to initialise not with random tensors, but with the tensors resulting from zero transverse field directly in a proper superposition $|\psi^\pm\rangle$ (referring to Eq. 3.2). To get a better insight in border and finite size influences, a comparison to solutions obtained from infinite size algorithms and to PBC would be sufficient but unfortunately could not be investigated further due to time limitations. For the sake of completeness, the antiferromagnetic case has been attached in Fig. 24.

¹ This run had an elapsed time of ≈ 10 h

3.2 BILINEAR BIQUADRATIC SPIN-1 CHAIN

The bilinear biquadratic spin-1 Hamiltonian with local interaction terms

$$H = \sum_{j=1}^{L-1} \alpha \mathbf{S}_j \mathbf{S}_{j+1} + \beta (\mathbf{S}_j \mathbf{S}_{j+1})^2 \quad (3.8)$$

yields a very rich phase diagram. It is common to write the coefficients $\alpha = \cos(\theta)$, and $\beta = \sin(\theta)$ in order to describe the system's Hamiltonian only with a systemwide parameter θ .

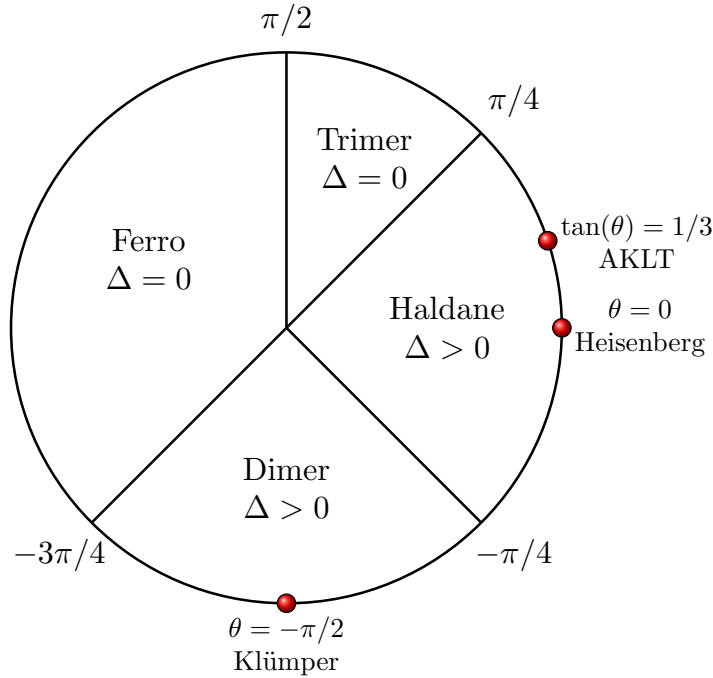


Figure 21: Phase chart for different values of θ . Δ represents the energy gap.

Notice that $\mathbf{S}_j \mathbf{S}_{j+1} = S_j^x S_{j+1}^x + S_j^y S_{j+1}^y + S_j^z S_{j+1}^z$ is a dot product of the composed spin-vectors $\mathbf{S}_j^T = (S_j^x, S_j^y, S_j^z)^T$. The BLBQ Hamiltonian contains a gapless ferromagnetic phase and an antiferromagnetic interval with trimer, Haldane and dimer phase. The Haldane phase can be found for $\theta \in [-\pi/4, \pi/4]$ and is expected to contain systems with unique ground state and finite excitation gap. Important points are the AKLT point for $\tan(\theta) = 1/3$, where the ground state energy can be given analytically [1] and the Heisenberg model for $\theta = 0$. Ferromagnetics can be found in the interval for $\theta \in [\pi/2, 5\pi/2]$. The pure biquadratic Hamiltonian for $\theta = -\pi/2$ has been solved by Klümper et al. [8].

The Hamilton of Eq. 3.8 can be reduced to

$$H = \left(\cos(\theta) - \frac{\sin(\theta)}{2} \right) \mathbf{S}_i \mathbf{S}_j + \sin(\theta) \left(\mathbf{V}_i \mathbf{V}_j + \frac{1}{2} \mathbf{W}_i \mathbf{W}_j \right), \quad (3.9)$$

with $\begin{cases} V_i^\alpha = S_i^{\alpha 2} \\ W_i^\gamma = \{S_i^\alpha, S_i^\beta\} \end{cases}$,

which then takes the form in local MPOs according to Fig. 22.

1  1 $\mathbb{1}_{3 \times 3} = \begin{pmatrix} 1 & 0 & 0 \\ 0 & 1 & 0 \\ 0 & 0 & 1 \end{pmatrix}$	1  8 $\frac{\beta}{2} W_x = \frac{\beta}{2\sqrt{2i}} \begin{pmatrix} 0 & 1 & 0 \\ -1 & 0 & -1 \\ 0 & 1 & 0 \end{pmatrix}$	5  11 V_x
1  2 $(\alpha - \frac{\beta}{2}) S_x = \frac{(\alpha - \frac{\beta}{2})}{\sqrt{2}} \begin{pmatrix} 0 & 1 & 0 \\ 1 & 0 & 1 \\ 0 & 1 & 0 \end{pmatrix}$	1  9 $\frac{\beta}{2} W_y = \frac{\beta}{2\sqrt{2}} \begin{pmatrix} 0 & 1 & 0 \\ 1 & 0 & -1 \\ 0 & -1 & 0 \end{pmatrix}$	6  11 V_y
1  3 $(\alpha - \frac{\beta}{2}) S_y = \frac{(\alpha - \frac{\beta}{2})}{\sqrt{2i}} \begin{pmatrix} 0 & 1 & 0 \\ -1 & 0 & 1 \\ 0 & -1 & 0 \end{pmatrix}$	1  10 $\frac{\beta}{2} W_z = \frac{\beta}{2i} \begin{pmatrix} 0 & 0 & 1 \\ 0 & 0 & 0 \\ -1 & 0 & 0 \end{pmatrix}$	7  11 V_z
1  4 $(\alpha - \frac{\beta}{2}) S_z = (\alpha - \frac{\beta}{2}) \begin{pmatrix} 1 & 0 & 0 \\ 0 & 0 & 0 \\ 0 & 0 & -1 \end{pmatrix}$	1  11 ΓS_z	8  11 W_x
1  5 $\beta V_x = \frac{\beta}{2} \begin{pmatrix} 1 & 0 & 1 \\ 0 & 2 & 0 \\ 1 & 0 & 1 \end{pmatrix}$	2  11 S_x	9  11 W_y
1  6 $\beta V_y = \frac{\beta}{2} \begin{pmatrix} 1 & 0 & -1 \\ 0 & 2 & 0 \\ -1 & 0 & 1 \end{pmatrix}$	3  11 S_y	10  11 W_z
1  7 $\beta V_z = \frac{\beta}{2} \begin{pmatrix} 2 & 0 & 0 \\ 0 & 0 & 0 \\ 0 & 0 & 2 \end{pmatrix}$	4  11 S_z	11  11 $\mathbb{1}_{3 \times 3}$

Figure 22: Local terms of the anisotropic bilinear-biquadratic spin-1 Hamiltonian. Note that the reduction to eq. 3.9 reduces the dimension of the local Hamiltonian to 11×11 . All other terms - those who are not explicitly assigned in this figure - are zero.

3.2.1 $\theta = \arctan(1/3)$ - The AKLT Point

According to chapter 2.4, a direct comparison of the variational approach and the AKLT state is possible. The ground state energy can be calculated with the AKLT tensors analogue to the observables for MPS

$$E_0 = \frac{\langle \psi_{\text{AKLT}} | H | \psi_{\text{AKLT}} \rangle}{\langle \psi_{\text{AKLT}} | \psi_{\text{AKLT}} \rangle}. \quad (3.10)$$

As expected, in order to receive an acceptable accuracy, a high bond dimension is unnecessary.

One observes that even for $m = 2$ the mean deviation is $\mathcal{O}(10^{-12})$, as predicted by the exact construction. For the AKLT point, at each site j the tensors are equal, hence the entanglement entropy should be constant for each subsystem size L_{left} , the offset dependent of the normalisation condition. In addition, the spectrum should consist of doubly degenerated singular values $\frac{1}{\sqrt{2}}$.

m	ΔEnergy
2	$1.665\,45 \times 10^{-12}$
20	$2.220\,45 \times 10^{-16}$
50	$2.220\,45 \times 10^{-16}$

Table 1: Energy difference obtained from AKLT and DMRG tensors at $L = 100$.

3.2.2 $\theta = 0$ - The Heisenberg Point

The isotropic antiferromagnetic spin-1 Heisenberg chain is the simplest example of a system with Haldane phase and thus often called the Haldane chain. For the isotropic case at $\theta = 0$ and $\Gamma = 0$, the Hamiltonian takes the Heisenberg form

$$H = -J \sum_{j=1}^{L-1} \mathbf{S}_j \mathbf{S}_{j+1}. \quad (3.11)$$

For spin-1/2, this can be exactly solved by approaching a *Bethe ansatz*. This is not possible for spin-1, therefore the numerical solution becomes very interesting to analyse properties that may differ from the spin-1/2 Heisenberg model according to Haldane's suggestion from 1983, that there has to be a fundamental difference between spin-1/2 and spin-1. This suggestion was not intuitive, because the derived solutions seemed to be appropriate for all spins. Stephen White et al. showed the power of DMRG with calculating some expectation values for the Haldane chain. This reference energy value has been obtained with the infinite lattice method - where the system length is increased until convergence for a fixed bond dimension is reached [20]. Also, White et al. removed the inconvenient degeneracy to exclude effects of the bulk by a chain construction with real spin-1/2 particles at the border. In order to receive a result with best uniformly distributed energy per site, he also varied the coupling at the chain ends. This has not been implemented in the DMRG here and has to be considered carefully for the following comparison.

The value for the energy per site $\langle S_i^x S_{i+1}^x \rangle + \langle S_i^y S_{i+1}^y \rangle + \langle S_i^z S_{i+1}^z \rangle$ has been recorded for $m = 50$ and $L = 100$ at the very centre of the chain, because border effects at the centre are minimal (see attachment, Fig. 30). In order to estimate the significant numbers - outside the brackets () - the same has been calculated for $L = 90$ and $L = 110$.

L	E_0
90	-1.401 483 485 119 951
100	-1.401 484 125 904 029
110	-1.401 485 506 786 237

Table 2: Energy per site for the Haldane chain. To estimate the significant numbers for $L = 100$, $L = 90$ and $L = 110$ have been recorded, aswell.

$$\begin{aligned}
E_0 &= -1.401\,48(4) \\
E_{0,\text{ref.}} &= -1.401\,484\,038\,971(4)
\end{aligned}
\tag{3.12}$$

Yet this comparison is not sufficient. For a total comparison, the limits for both $m \rightarrow \infty$ and $L \rightarrow \infty$ have to be taken, e.g. by iteratively rising m and then L . The result is estimated to be reasonable considering that it is not obtained from an infinite site and infinite bond dimension measurement.

3.2.3 $\theta = -\pi/2$ - The Klümper Point

The Klümper Hamiltonian can be written in terms of spin projection operators P_j in an analogue way to the AKLT Hamiltonian (see Eq. 2.28)

$$H_{\text{Klümper}} = -3P_0 - \mathbb{1} . \tag{3.13}$$

Since there cannot be a singlet on every link, the phase is dimerised. For even system sizes L , there is only a unique configuration for the ground state. For odd system sizes, there are two energetically equal dimer states hence for the superposition every bond becomes equal, too. These two different cases are noticeable in the entanglement spectrum for even and odd system sizes L (see Fig. 23).

3.2.4 Entanglement Spectrum at different Phase Points

The entanglement spectrum provides a way to analyse the quantum mechanical structure of entangled states. For the AKLT state, the spectrum is doubly degenerate, which is a direct consequence of the maximally entangled virtual spin-1/2. In a similar way, an analysis of singular values is a direct check, if a toy model seems plausible or not. Also, it may be a new idea to define a phase [13], since global quantities like string order turn out to be insufficient under perturbations or deformations of the Hamiltonian. For the Haldane phase exists some structure of virtual spin subcomponents and the bonds between each site are equal. Moreover, the doubly degenerate highest singular value can be found in the entire Haldane chain (see Fig.: 23). This is associated to *symmetry protected topological order* [14], which means that there is a long-range entanglement pattern protected by symmetries in this phase. This also implies that the entanglement spectrum gives an idea of what are the physical properties at the boundary. The fine splitting at some peculiar points (i.e. $-\arctan(1/3)$, $-1/2 \cdot \arctan(1/3)$, $2 \cdot \arctan(1/3)$) is caused by transition effects. The Klümper point is as expected for the highest singular values. Even though the upper spectrum can be seen in the figure, yet a detailed discussion would reach beyond the scope of this introductory thesis.

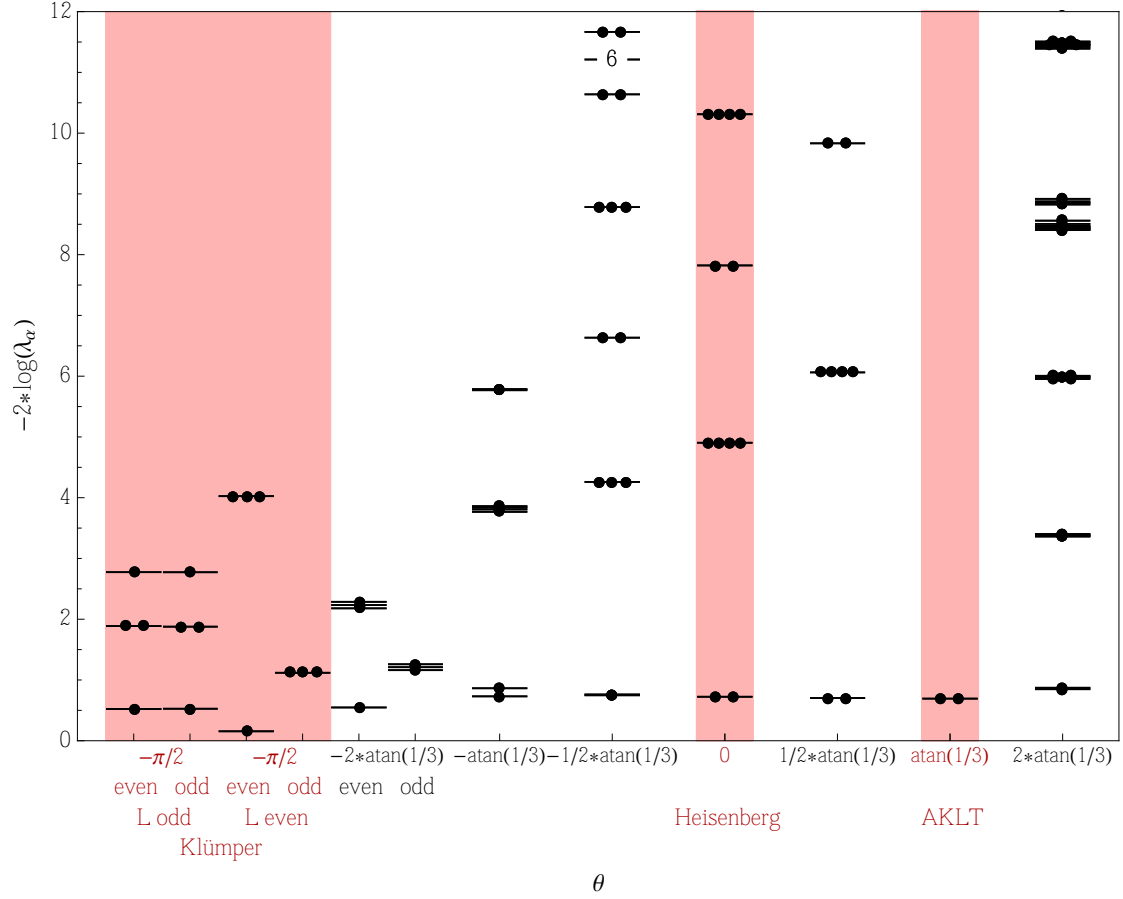


Figure 23: Entanglement spectrum at different points θ of the BLBQ phase diagram. The spectrum of the Klumper phase shows a difference between the even and odd bounds, because the model favours contractions of the real spin-1 to spin-0, hence neighbouring bonds differ in entanglement for even system sizes L . At $\theta = -1/2 \cdot \arctan(1/3)$ and $\theta = 2 \cdot \arctan(1/3)$, the highest *two* singular values are nearly degenerated. One can notice that the pattern of these two values is found in the entire Haldane phase.

SUMMARY AND OUTLOOK

In this thesis, the basics of matrix product states and the density matrix renormalisation group under a quantum information perspective have been allocated. The main aspects to implement a reformulated DMRG have been provided and can be used as instructions to code an own programme. Especially the attached code should be helpful to do so.

A review of existing results and the comparison gave us a deeper understanding of what it is good for. An insight in the Ising and BLBQ model has been given to understand the practical relevance of MPS approaches. Within the demonstration chapter, we have seen an area law for the critical Ising model. For the BLBQ Hamiltonian, the AKLT and Klümper points have been analysed both analytically and numerically. The numerical value for the energy per site of the Haldane chain has been checked.

We learned, that the main purpose of the MPS formalism is not only the effective reconstruction of a systems ground state. It can be used to analyse a system's deepest structure and to quantify its entanglement or particular local quantities. Moreover, it provides techniques to search for quantities that redefine the understanding of a phase.

Since a symmetry breaking, border and finite size effects have been noticed, they have to be reviewed more intense in future work.

We hope, that this thesis provides a basic introduction in the field of one dimensional MPS approaches.

ACKNOWLEDGMENT

I would like to thank my supervisor Matteo Rizzi for the intuitive way to enter the huge field of quantum information and especially the formalism of matrix product states barely without any background knowledge. Thank you for the huge amount of time that you spend with me during my thesis and for the patient way of answering my countless questions. Special thanks to Román Orús, who co-supervised this work and enlightened a lot of arised misunderstandings. Last, but not least thanks to Johannes Jünemann for the many inspiring discussions and the correction of this thesis. I really enjoyed the atmosphere in this group and wish you all the best for the future.

APPENDIX A - PROGRAMME CODE

A.1 AKLT MODEL

This programme has been implemented for getting used to MatLab and review the motivation for the AKLT matrices. Running this file yields only two nonzero Schmidt coefficients for each S_1, S_2, S_3 . The same states can be reproduced - modulo norm of the state - by contracting the AKLT matrices. Be careful - the superposition state is not been given directly yet needs to be constructed via a sum/difference of the correct states.

```

1  %% Spin 1 Particles at Latticepoints of a 1D Chain
   % spin 1 operators
   %-----
   S = zeros(3,3,3);
6  Sx = [0 1 0 ; 1 0 1 ; 0 1 0]*1/sqrt(2);
   Sy = [0 1 0 ; -1 0 1 ; 0 -1 0]*1/(sqrt(2)*i);
   Sz = [1 0 0 ; 0 0 0 ; 0 0 -1];
   S(:,:,1) = Sx;
11  S(:,:,2) = Sy;
   S(:,:,3) = Sz;
   Dim_S=3;
   J = 3;

   % system length, boundary condition
16  %-----
   L=4;
   BC = 'OBC';
   alpha = 1/3;

21  % hilbert space dimension
   %-----
   Dim_H = Dim_S*L;

   % system spin matrix
26  %-----
   S_H = zeros(Dim_H,Dim_H,L,J);

   %% Spin Loop

31  % loop over x,y,z
   %-----
   for j=1:J
       % loop over all points
       for l=1:L
36         tp=1;
           % correct position of the 3x3 S_j matrix in tensor product chain
           for i=1:L
               if i==1
41                 tp = kron(S(:,:,j),tp);
               else
                   tp = kron(eye(Dim_S),tp);
               end
           end
           % tp is now the S_lj component of the total spin operator
46         % and saved in S_H
           S_H(:,:,l,j) = tp;
       end
   end
   clear tp j l i S_j

51  %% Constructing the Hamiltonian

   H = zeros(Dim_H);
   if BC == 'OBC'
56     L_BC = L-1;
   else if BC == 'PBC'
       L_BC = L;
   end

```

```

        else disp('Check Boundary Conditions');
        end
61 end

for l=1:L_BC
    tp1 = zeros(Dim_H);
    tp2 = zeros(Dim_H);
66     for j=1:3
        % add up S_l*S_(l+1) component by component j
        if l == L
            tp1 = tp1 + S_H(:,:,l,j)*S_H(:,:,l,j);
        else
71             tp1 = tp1 + S_H(:,:,l,j)*S_H(:,:,l+1,j);
            end
        end
        tp2 = alpha*tp1^2;
        H = H + tp1 + tp2;
76 end
H = sparse(1/2*(H + conj(H')));
clear j l tp1 tp2 L_BC

%% diagonal form of H
81 % find ONB of H
[Evec_H, Eval_H] = schur(full(H));
% sort Eval and Evec of H the same way
[Eval_H, Order_EvalH] = sort(diag(Eval_H));
86 Evec_H = Evec_H(:, Order_EvalH);
% degeneracy of ground state energy
Deg_H = nnz(abs(Eval_H - Eval_H(1)) < 1e-12);
G = Evec_H(:, 1:Deg_H);

91 %% Constructing the Total Spin Operator

S_T = zeros(Dim_H, Dim_H, J);
% construction S_T component by component
%-----
96 for j=1:J
    % S_Tj is a square dim_H matrix
    S_Tj = zeros(Dim_H);
    % sum over the lattice points
    for l=1:L
101         S_Tj = S_Tj + S_H(:,:,l,j);
        end
        S_T(:,:,j) = S_Tj;
    end
clear j l

106 S_Tsq = zeros(Dim_H);
for j=1:J
    S_Tsq = S_Tsq + (S_T(:,:,j))^2;
end
111 clear j l

% symmetrical machine errors
%-----
S_Tsq = 1/2 * (S_Tsq + conj(S_Tsq'));
116 S_Tz = 1/2 * (S_T(:,:,3) + conj(S_T(:,:,3)'));

[Evec_STsq, Eval_STsq] = schur(G'*S_Tsq*G);
Eval_STsq = diag(Eval_STsq);

121 %% Entangled E0 Spin States

% the ONB of S_T & H: a projection of G to the S_T subspace of H
%-----

126 % [S_Tsq, S_Tz] != 0
% find entries of entangled s = 2 states
Deg_STsq = find(abs(Eval_STsq - 2) < 1e-10);
Deg_EvecSTsq = G * Evec_STsq(:, Deg_STsq);
[Evec_STz, Eval_STz] = schur(Deg_EvecSTsq'*S_Tz*Deg_EvecSTsq);
131 G = G * Evec_STsq;
% first state is a not degenerated s=0 spin state;
G(2:Dim_H, Deg_STsq) = G(2:Dim_H, 2:Deg_H)*Evec_STz;

% spin measurement
%-----
136 Proj_Ssz = zeros(2,4);
for s=1:Deg_H
    Proj_Ssz(1,s) = G(:,s)'*S_Tsq*G(:,s);
    Proj_Ssz(2,s) = G(:,s)'*S_Tz*G(:,s);
141 end
clear s

```

```

%% Building the Tensor Network (|1 -1> State)
146 % sequential svd
%-----
MPS_Class = zeros(L,Dim_S,Dim_S,Dim_S,Dim_S);
Gamma_1 = zeros(L,Dim_S,Dim_S);
Gamma_2 = zeros(L,Dim_S,Dim_S,Dim_S^2);
151 Gamma_3 = zeros(L,Dim_S^2,Dim_S,Dim_S);
Gamma_4 = zeros(L,Dim_S,Dim_S);

for State=1:4
    KetSSz = reshape(G(:,State),[Dim_S,Dim_S^(L-1)]);
156 [U_1,S_1,V_1] = svd(full(KetSSz),'econ');
Gamma_1(State,:,:) = reshape(U_1,[Dim_S,Dim_S]);
W_1 = S_1*V_1';
W_1r = reshape(W_1,[Dim_S^2,Dim_S^2]);
[U_2,S_2,V_2] = svd(W_1r,'econ');
161 Gamma_2(State,:,:) = reshape(U_2,[Dim_S Dim_S Dim_S^2]);
W_2 = S_2*V_2';
W_2r = reshape(W_2,[Dim_S^3,Dim_S]);
[U_3,S_3,V_3] = svd(W_2r,'econ');
166 Gamma_3(State,:,:) = reshape(U_3,[Dim_S^2 Dim_S Dim_S]);
W_3 = S_3*V_3';
Gamma_4(State,:,:) = W_3;
S_1 = diag(S_1);
S_2 = diag(S_2);
171 S_3 = diag(S_3);
Trash = 10^-10;

Gamma_1(abs(Gamma_1) < Trash) = 0;
Gamma_2(abs(Gamma_2) < Trash) = 0;
176 Gamma_3(abs(Gamma_3) < Trash) = 0;
Gamma_4(abs(Gamma_4) < Trash) = 0;

MPS_Classr = reshape(permute(MPS_Class,[2:(L+1),1]),[Dim_H,L]);
clear i j k l
end
181

%% TN Construction with the AKLT Model

% Pauli matrices
%-----
186 sig_x = [0 1 ; 1 0];
sig_y = [0 -i ; i 0];
sig_z = [1 0 ; 0 -1];
Dim_P = 2;

191 % ladder operators
%-----
sig_p = 1/2*(sig_x + i*sig_y);
sig_m = 1/2*(sig_x - i*sig_y);

196 % AKLT operators
%-----
A = zeros(2,3,2);
A(:,1,:) = sig_p;
201 A(:,2,:) = -sig_z/sqrt(2);
A(:,3,:) = -sig_m;

% state construction
%-----
206 MPS_AKLT = zeros(Dim_P,Dim_S,Dim_S,Dim_S,Dim_S,Dim_P);
for alpha = 1:Dim_P
    for j = 1:Dim_S
        for k = 1:Dim_S
            for l = 1:Dim_S
                for m = 1:Dim_S
                    for beta = 1:Dim_P
211 MPS_AKLT(alpha,j,k,l,m,beta) = MPS_AKLT(alpha,j,k,l,m,beta)...
+ reshape(A(alpha,j,:),[1,Dim_P])...
*reshape(A(:,k,:),[Dim_P,Dim_P])...
*reshape(A(:,l,:),[Dim_P,Dim_P])...
216 *A(:,m,beta);
                    end
                end
            end
        end
    end
221 end

clear alpha j k l m beta
MPS_AKLT = reshape(permute(MPS_AKLT,[2:(L+1) 1 (L+2)]),[Dim_H,L]);

```

A.2 VARIATIONAL APPROACH

This file is the implemented MPS approach. The resulting two MPS are a left canonical ACanLQ,ACanLR system with QRD optimalvectors and right canonical ACanRQ,ACanRR. The output is energy per site after each optimisation step and a comparison to the previous optimisation in order to check the convergence.

```

5  %% Energy Optimisation
   % DMRG Algorithm for Energy Optimisation.
   % This file provides after each step a total right and a total left
   % canonical MPS, which consists of optimal tensors, received from the
   % determination of eigenvalues and vectors for the effective hamiltonian.

10  % calculate computation time
   tic
   % global variables
   %-----
   global nbond m n d L
   InitialValues;

15  % due to a change in physical dimension and MPD bond dimension
   %-----
   Size_MPOH = size(H);
   nbond = Size_MPOH(1);
   n = nbond*ones(1,L+1);

20  HR = cell(1,L+1);
   HL = cell(1,L);

25  % deal with borders: make a dirac delta for the first and last MPO
   % then every contraction becomes equal
   %-----
   DD = zeros(1,n(L),1);
   DD(1,n(L),1)=1;
   DD = reshape(DD,[m(L+1),n(L),m(L+1)]);
30  HR{L+1}=DD;
   clear DD
   DD = zeros(1,n(2),1);
   DD(1,1,1)=1;
   DD = reshape(DD,[m(1),n(2),m(1)]);
35  HL{1}=DD;
   clear DD

   % provides the initial right and left canonical MPS
   %-----
40  for j=L:-1:1
       HR = HRStep(HR,ACanRQ,j);
   end
   clear j
45  for j=1:L
       HL = HLStep(HL,ACanLQ,j);
   end
   clear j

50  % set a waitbar for progress visualisation
   %-----
   h1 = waitbar(0,'1','Name','Optimisation...','...
       'CreateCancelBtn','setappdata(gcf,'canceling','1)');
   setappdata(h1,'canceling',0);

55  EVec = cell(1,L);
   EVal = zeros(tns,2*L);
   % after the first sweep, startguesses are used
   %-----
60  startguessl = cell(1,L);
   for j=1:L
       startguessl{j} = rand([m(j)*m(j+1)*d(j),1]);
   end
   clear j

65  startguessr = cell(1,L);
   for j=1:L
       startguessr{j} = rand([m(j)*m(j+1)*d(j),1]);
   end
   clear j

70  for s=1:tns
       for j=1:L
           opts.v0=startguessl{j};
           % DMRG

```

```

75     [EVec{j}, EVal(s, j)] = eigs(@(X)(H_eff(HL, HR, j, X))...
        , m(j)*d(j)*m(j+1), 1, 'sr', opts);
        % startguess for next optimisation
        startguessl{j}=EVec{j};
80     % bringing the eigenvector in the right order
        EVec{j} = permute(reshape(EVec{j}, [m(j), d(j), m(j+1)]), [1, 3, 2]);
        % make the optimal tensor canonical
        [ACanLQ{j}, ~, ACanLR{j}, ~] = MakeCanonical(EVec{j}, 'L');
        % go with the left superblock to the next step
        HL = HLStep(HL, ACanLQ, j);
85     % waitbar stuff
        % -----
        if getappdata(h1, 'canceling')
            delete(h1)
            break
90     end
        waitbar(j/(L-1), h1, ['sweep ', num2str(s), '/', num2str(tns)])
    end
    clear j
    for j=L:-1:1
95         opts.v0 = startguessr{j};
            [EVec{j}, EVal(s, L+j)] = eigs(@(X)(H_eff(HL, HR, j, X)), m(j)*m(j+1)*d(j), 1, 'sr', opts);
            startguessr{j}=EVec{j};
            EVec{j} = permute(reshape(EVec{j}, [m(j), d(j), m(j+1)]), [1, 3, 2]);
            [~, ACanRQ{j}, ~, ACanRR{j}] = MakeCanonical(EVec{j}, 'R');
100         HR = HRStep(HR, ACanRQ, j);
            % waitbar stuff
            % -----
            if getappdata(h1, 'canceling')
                delete(h1)
                break
105         end
            waitbar(j/(L-1), h1, ['sweep ', num2str(s), '/', num2str(tns)])
        end
        if s > 1 && EVal(s, L) < EVal(s-1, L)
110         disp(['sweep ', num2str(s), ' optimisation successful ', num2str(EVal(s, L)/L)])
        elseif s > 1 && EVal(s, L) - EVal(s-1, L) <= 1e-12
            disp(['sweep ', num2str(s), ' threshold ', num2str(EVal(s, L)/L)])
        elseif s > 1 && EVal(s, L) > EVal(s-1, L)
            disp(['sweep ', num2str(s), ' error: ', num2str(EVal(s, L)/L)])
115     end
    end
    clear s

    delete(h1)
120    toc

```

The next list is the code for the calculation of expectation quantities of a MPO with the set of canonical MPS A and their corresponding R matrix after QRD.

```

function Obs = EV_Obs(A, R, MPO, dir)

global m d L

5 Size_MPO = size(MPO);
  nbond = Size_MPO(1);

  n = nbond*ones(1, L+1);

10 if strcmp(dir, 'LR')
    MPOL = cell(1, L+2);
    DD = zeros(1, n(2), 1);
    DD(1, 1, 1)=1;
    DD = reshape(DD, [m(1), n(1), m(1)]);
15 MPOL{1}=DD;
    clear DD

    DD = zeros(1, n(L), 1);
    DD(1, n(L), 1)=1;
20 DD = reshape(DD, [m(L+1), n(L+1), m(L+1)]);
    MPOL{L+2}=DD;
    clear DD
    for j=1:L
        % (L-R) direction
        %-----
25         % Contraction 1 (HL, MPS)
            Dt = reshape(permute(MPOL{j}, [2, 3, 1]), [n(j)*m(j), m(j)])*reshape(A{j}, [m(j), m(j+1)*d(j)]);
            D = permute(reshape(Dt, [n(j), m(j), m(j+1), d(j)]), [3, 4, 1, 2]);
            % Contraction 2 ((HL, MPS), MPO)
30         Et = reshape(permute(D, [1, 4, 2, 3]), [m(j+1)*m(j), d(j)*n(j)])*reshape(permute(MPO, [3, 1, 2, 4]), [d(j)*n(j), n(j)+1]*d(j));
            E = permute(reshape(Et, [m(j+1), m(j), n(j+1), d(j)]), [1, 3, 4, 2]);
            % Contraction 3 ((HL, MPS), MPO), MPS)
            Ft = reshape(E, [m(j+1)*n(j+1), d(j)*m(j)])*reshape(permute(conj(A{j}), [3, 1, 2]), [d(j)*m(j), m(j+1)]);

```

```

35     C = reshape(Ft,[m(j+1),n(j+1),m(j+1)]);
        MPOL{j+1} = C;
    end
    clear Dt D Et E Ft C
    % Contraction 4 (((HL, MPS), MPO), MPS),HL{L+2}}
40     MPOL{L+2} = MPOL{L+1}*(R*R')*MPOL{L+2}';
    Obs = MPOL{L+2};

    elseif strcmp(dir,'RL')
        MPOR = cell(1,L+2);
45     DD = zeros(1,n(L+1),1);
        DD(1,n(L+1),1)=1;
        DD = reshape(DD,[m(L+1),n(L+1),m(L+1)]);
        MPOR{L+2}=DD;
        clear DD

50     DD = zeros(1,n(L),1);
        DD(1,1,1)=1;
        DD = reshape(DD,[m(L+1),n(L),m(L+1)]);
        MPOR{1}=DD;
55     clear DD
        for j=L:-1:1
            % (R-L) direction
            %-----
            % Contraction 1 MPS, HR
60     Dt = reshape(permute(A{j},[1,3,2]),[m(j)*d(j),m(j+1)])*reshape(MPOR{j+2},[m(j+1),n(j+1)*m(j+1)]);
                D = reshape(Dt,[m(j),d(j),n(j+1),m(j+1)]);
                % Contraction 2 ..., MPO
                Et = reshape(permute(D,[1,4,2,3]),[m(j)*m(j+1),d(j)*n(j+1)])*reshape(permute(MPO,[3,2,1,4]),[d(j)*n(j+1),
                    n(j)*d(j)]);
                E = permute(reshape(Et,[m(j),m(j+1),n(j),d(j)]),[1,3,4,2]);
65     % Contraction 3 ..., MPS*
                Ft = reshape(conj(permute(A{j},[1,3,2]),[m(j),d(j)*m(j+1)])*reshape(permute(E,[3,4,1,2]),[d(j)*m(j+1),m(
                    j)*n(j)]);
                C = permute(reshape(Ft,[m(j),m(j),n(j)]),[2,3,1]);

                MPOR{j+1} = C;
70     end
        MPOR{1} = MPOR{1}*MPOR{2}';
        Obs = MPOR{1};
        end
75     end

```

In the following one can see the calculation of correlation values. The point is, that - assuming $j > i$ - only the contraction from i to j contributes to the final value (normalisation). After site j , the chain may be closed with the contraction of R and R^\dagger from the QRD of the optimum eigenvector.

```

function Obs = EV_Corr(A,R,MPO,MPOCorr,pos1,pos2)

global m d L

5     Size_MPO = size(MPO);
    nbond = Size_MPO(1);

    n = nbond*ones(1,L+1);

10    if pos2>=pos1
        elseif pos1>pos2
            tp=pos2;
            pos2=pos1;
            pos1=tp;
            clear tp
15    end

    MPOL = cell(1,L+2);
    MPOL{pos1} = reshape(eye(m(pos1),m(pos1)),[m(pos1),n(pos1),m(pos1)]);
20    for j=pos1:pos2
        % (L-R) direction
        %-----
        % Contraction 1 (HL, MPS)
        Dt = reshape(permute(MPOL{j},[2,3,1]),[n(j)*m(j),m(j)])*...
            reshape(A{j},[m(j),m(j+1)*d(j)]);
25     D = permute(reshape(Dt,[n(j),m(j),m(j+1),d(j)]),[3,4,1,2]);
            % Contraction 2 ((HL, MPS), MPO)
            if j==pos1||j==pos2
                Et = reshape(permute(D,[1,4,2,3]),[m(j+1)*m(j),d(j)*n(j)])*...
30             reshape(permute(MPOCorr,[3,1,2,4]),[d(j)*n(j),n(j+1)*d(j)]);
            else
                Et = reshape(permute(D,[1,4,2,3]),[m(j+1)*m(j),d(j)*n(j)])*...

```

```

    reshape(permute(MPO,[3,1,2,4]),[d(j)*n(j),n(j+1)*d(j)]);
end
35 E = permute(reshape(Et,[m(j+1),m(j),n(j+1),d(j)]),[1,3,4,2]));
    % Contraction 3 ((HL, MPS), MPO), MPS
Ft = reshape(E,[m(j+1)*n(j+1),d(j)*m(j)])*...
    reshape(permute(conj(A{j}),[3,1,2]),[d(j)*m(j),m(j+1)]);
40 C = reshape(Ft,[m(j+1),n(j+1),m(j+1)]);
    MPOL{j+1} = C;
end
clear Dt D Et E Ft C
Obs = trace(conj(R{pos2})*reshape(MPOL{pos2+1},[m(pos2+1),m(pos2+1)])...
    *R{pos2});
45 end

```

The next two auxiliary functions successively contract the right and left side of the effective Hamiltonian.

```

function [HL] = HLStep(HL,A,j)
global m n d H
    % (L-R) direction
    %-----
4   % Contraction 1 (HL, MPS)
    Dt = reshape(permute(HL{j},[2,3,1]),[n(j)*m(j),m(j)])*reshape(A{j},[m(j),m(j+1)*d(j)]);
    D = permute(reshape(Dt,[n(j),m(j),m(j+1),d(j)]),[3,4,1,2]);
    % Contraction 2 ((HL, MPS), MPO)
9   Et = reshape(permute(D,[1,4,2,3]),[m(j+1)*m(j),d(j)*n(j)])*reshape(permute(H,[3,1,2,4]),[d(j)*n(j),n(j+1)*d(j)]);
    E = permute(reshape(Et,[m(j+1),m(j),n(j+1),d(j)]),[1,3,4,2]);
    % Contraction 3 ((HL, MPS), MPO), MPS
    Ft = reshape(E,[m(j+1)*n(j+1),d(j)*m(j)])*reshape(permute(conj(A{j}),[3,1,2]),[d(j)*m(j),m(j+1)]);
    C = reshape(Ft,[m(j+1),n(j+1),m(j+1)]);
14  HL{j+1} = C;
end

```

```

function [HR] = HRStep(HR,A,j)
global m n d H
    % (R-L) direction
    %-----
4   % Contraction 1 MPS, HR
    Dt = reshape(permute(A{j},[1,3,2]),[m(j)*d(j),m(j+1)])*reshape(HR{j+1},[m(j+1),n(j+1)*m(j+1)]);
    D = reshape(Dt,[m(j),d(j),n(j+1),m(j+1)]);
    % Contraction 2 ..., MPO
9   Et = reshape(permute(D,[1,4,2,3]),[m(j)*m(j+1),d(j)*n(j+1)])*reshape(permute(H,[3,2,1,4]),[d(j)*n(j+1),n(j)*d(j)]);
    E = permute(reshape(Et,[m(j),m(j+1),n(j),d(j)]),[1,3,4,2]);
    % Contraction 3 ..., MPS*
    Ft = reshape(conj(permute(A{j},[1,3,2]),[m(j),d(j)*m(j+1)])*reshape(permute(E,[3,4,1,2]),[d(j)*m(j+1),m(j)*n(j)]);
14  C = permute(reshape(Ft,[m(j),m(j),n(j)]),[2,3,1]);
    HR{j} = C;
end

```

APPENDIX B - MATHEMATICAL TOOLS

B.1 SCHMIDT DECOMPOSITION

Theorem

Let

$$|\psi_{A,B}\rangle \in \mathcal{H}_A \otimes \mathcal{H}_B, \quad |\psi_{A,B}\rangle = \sum_{i,j} \psi_{i,j} |i\rangle_A |j\rangle_B . \quad (\text{B.1})$$

There is always a decomposition

$$|\psi_{A,B}\rangle = \sum_{\alpha}^m \lambda_{\alpha} |\alpha\rangle_A |\alpha\rangle_B , \quad (\text{B.2})$$

with $m = \min(\dim(\mathcal{H}_A), \dim(\mathcal{H}_B))$, $\langle \alpha | \alpha' \rangle_A = \langle \alpha | \alpha' \rangle_B = \delta_{\alpha\alpha'}$, which means there is an orthonormal basis of \mathcal{H}_A and \mathcal{H}_B .

Proof

ψ can be decomposed via SVD to $\psi = U\Lambda V^{\dagger}$

$$\Rightarrow \psi_{i,j} = \sum_{\alpha=1}^r U_{i\alpha} \Lambda_{\alpha\beta} (V^{\dagger})_{\beta j} = \sum_{\alpha=1}^r U_{i\alpha} \lambda_{\alpha} (V^{\dagger})_{\alpha j} . \quad (\text{B.3})$$

Inserting this in the state $|\psi_{A,B}\rangle$ yields

$$\begin{aligned} |\psi_{A,B}\rangle &= \sum_{i=1}^{d_A} \sum_{j=1}^{d_B} \sum_{\alpha=1}^r U_{i\alpha} \lambda_{\alpha} (V_{\alpha j}^{\dagger} |i\rangle_A |j\rangle_B) \\ &= \sum_{\alpha=1}^r \lambda_{\alpha} \underbrace{\left(\sum_{i=1}^{d_A} U_{i\alpha} |i\rangle_A \right)}_{\equiv |\alpha\rangle_A} \underbrace{\left(\sum_{j=1}^{d_B} V_{\alpha j}^{\dagger} |j\rangle_B \right)}_{\equiv |\alpha\rangle_B} \\ &= \sum_{\alpha=1}^r \lambda_{\alpha} |\alpha\rangle_A |\alpha\rangle_B . \end{aligned} \quad (\text{B.4})$$

Note

1. $|\alpha\rangle_A, |\alpha\rangle_B$ are called *Schmidt vectors*.
2. $m = 1 \Leftrightarrow |\psi_{A,B}\rangle$ is separable.
3. m is a measure of entanglement. The larger m is, the more entangled is the state.

B.2 QR DECOMPOSITION

SVD is a way to extract all needed information out of a given matrix, but very often one is only interested in orthogonality of U and the product of SV^T . Due to computation time optimisation, the QR decomposition is a numerically more efficient method, which for an arbitrary matrix M of dimension $(d_A \times d_B)$ yields a decomposition

$$M = QR. \tag{B.5}$$

Q is a left and right orthogonal square $(d_A \times d_A)$ and R is an upper triangular matrix $R_{ij} = 0$ for $i > j$.

APPENDIX C - MISCELLANEOUS

C.1 THE ISING MODEL AND ITS MAJORANA FORM

Starting from Eq. 3.1 with Pauli matrices instead of spin matrices, the \mathcal{Z}^2 symmetry is given by the parity operator

$$P_F = (-1)^{a_j^\dagger a_j} \quad (\text{C.1})$$

and the string like fermionic annihilation and creation operators (which correspond to the Jordan-Wiegener transformation)

$$\begin{aligned} a_j &= \left(\prod_{k<j} \sigma_k^z \right) \sigma_j^+ \\ a_j^\dagger &= \left(\prod_{k<j} \sigma_k^x \right) \sigma_j^- , \end{aligned} \quad (\text{C.2})$$

where σ_j^\pm are the spin ladder operators

$$\sigma_j^\pm = \sigma_j^x \pm i\sigma_j^y . \quad (\text{C.3})$$

They fulfill the (anti-) commutation relation

$$\{a_i, a_j^\dagger\} = \delta_{i,j} \quad a_i^2 = 0 \quad \{a_i, a_j\} = \{a_i^\dagger, a_j^\dagger\} = 0 . \quad (\text{C.4})$$

With this, the coupling term reads

$$S_{j,x} S_{j+1,x} = - \left(a_j - a_j^\dagger \right) \left(a_{j+1} + a_{j+1}^\dagger \right) . \quad (\text{C.5})$$

Putting this expressions in 2.47, the result is

$$H = \sum_{j=1}^{L-1} J \left(a_j - a_j^\dagger \right) \left(a_{j+1} + a_{j+1}^\dagger \right) - \sum_{j=1}^L \Gamma \left(a_j^\dagger a_j - \frac{1}{2} \mathbb{1} \right) . \quad (\text{C.6})$$

The Hamiltonian conserves the number of particles modulo 2 due to terms like $a_j a_{j+1}$. Majorana operators provide a sufficient way for a description of such systems. They are introduced via

$$\begin{aligned} c_{2j} &= -i \left(a_j - a_j^\dagger \right) , \\ c_{2j-1} &= a_j + a_j^\dagger , \\ a_j^\dagger a_j &= \frac{1}{2} \left(\mathbb{1} - i c_{2j} c_{2j-1} \right) \end{aligned} \quad (\text{C.7})$$

C.2 ADDITIONAL PLOTS

C.2.1 Ising Model

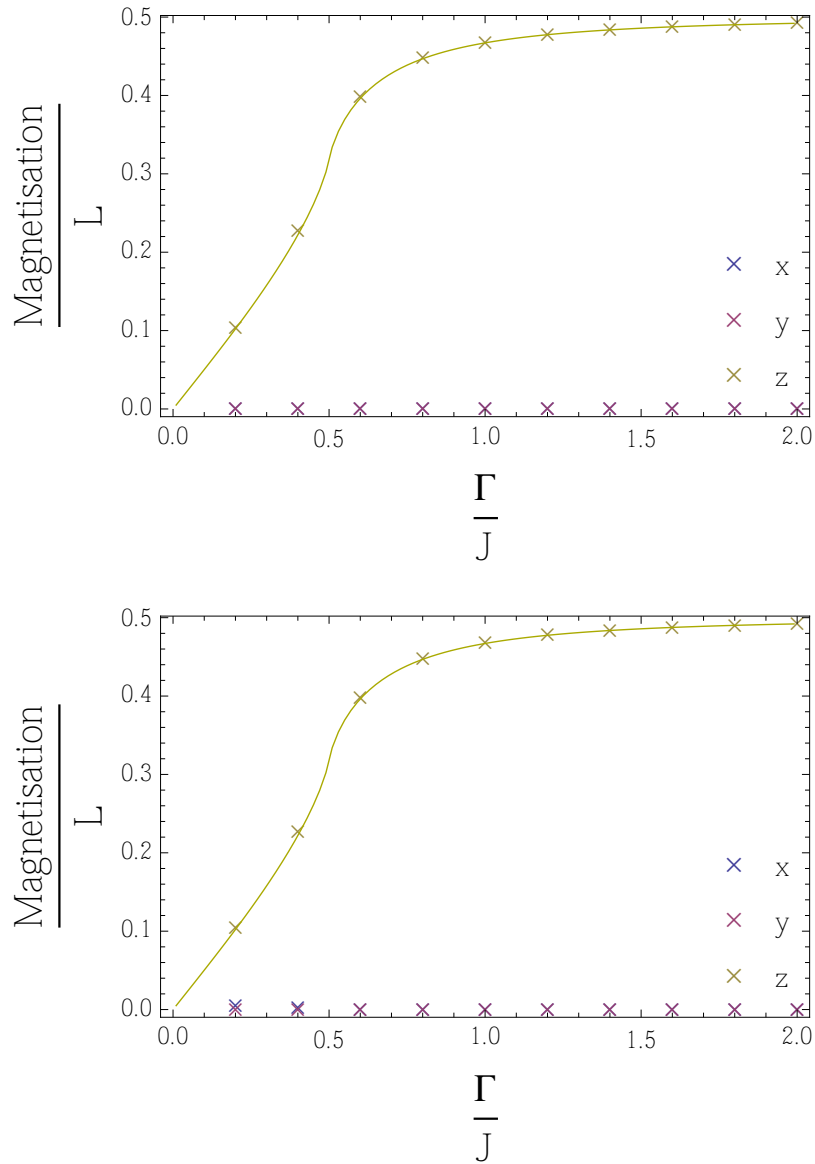


Figure 24: The antiferromagnetic case of the Ising model with an even (top) and odd (bottom) number of sites. The first value for the magnetisation in x direction is $\frac{M_x}{L} = 0.00438$ which corresponds to a total value $\approx \frac{1}{2}$ (not exactly because transverse field is nonzero). This is exactly the only lonely spin at the end of the chain, all others sum up to 0, therefore the order is $|\uparrow\downarrow\uparrow\downarrow \dots \uparrow\downarrow\rangle$.

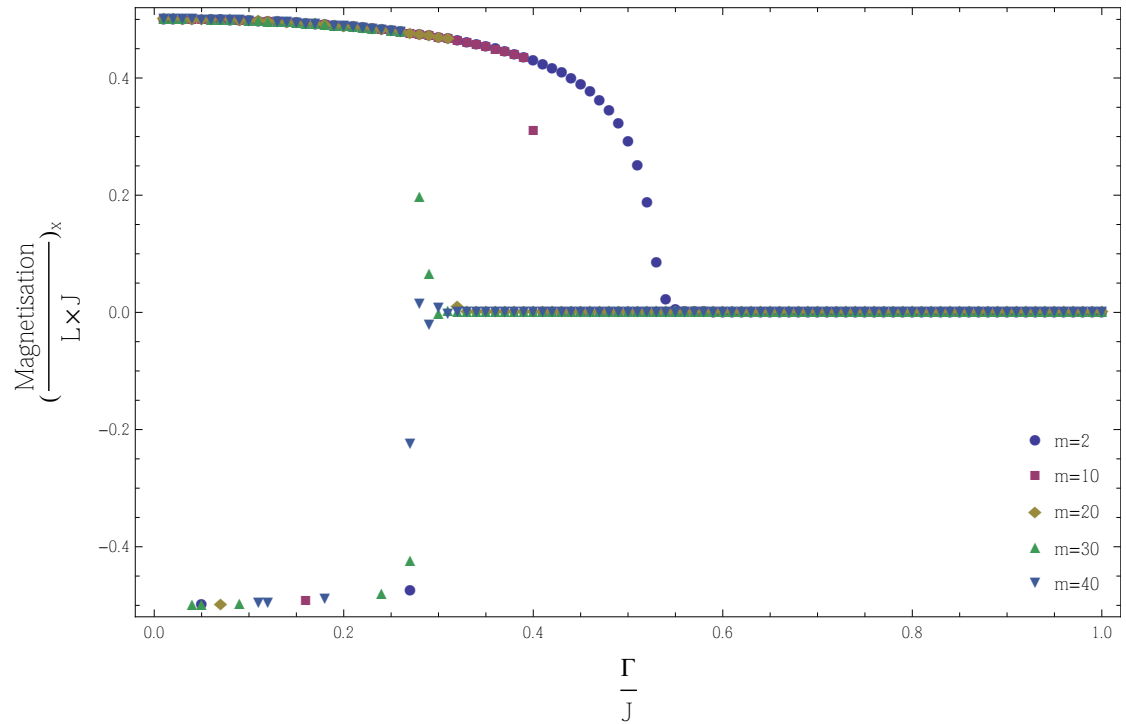


Figure 25: Change of the magnetisation along z -axis under change of bond dimension. Rising m , the numerical solution converges to the analytical with $M_x = 0 \forall \frac{\Gamma}{J} \neq 0$. The curve follows the analytical solution for PBC, which appears to be a symmetry break for nonzero transverse field.

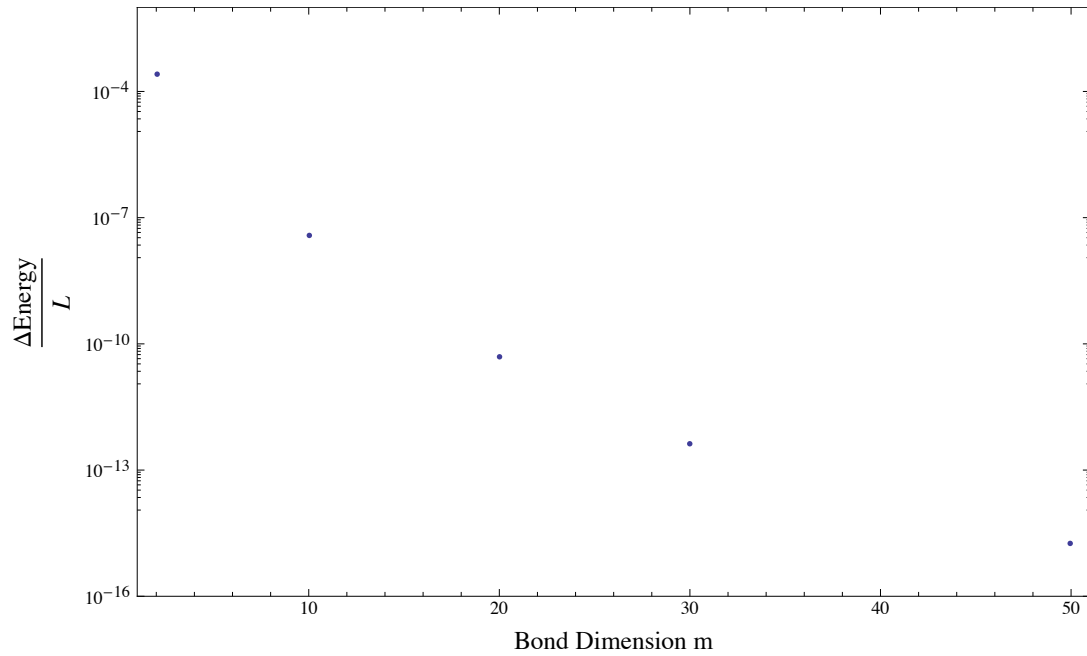


Figure 26: Energy convergence vs m at the pure ferromagnetic case $\Gamma = 0$. As expected, when the bond dimension is increased, the accuracy is increased, because more entanglement is considered.

C.3 AKLT MODEL

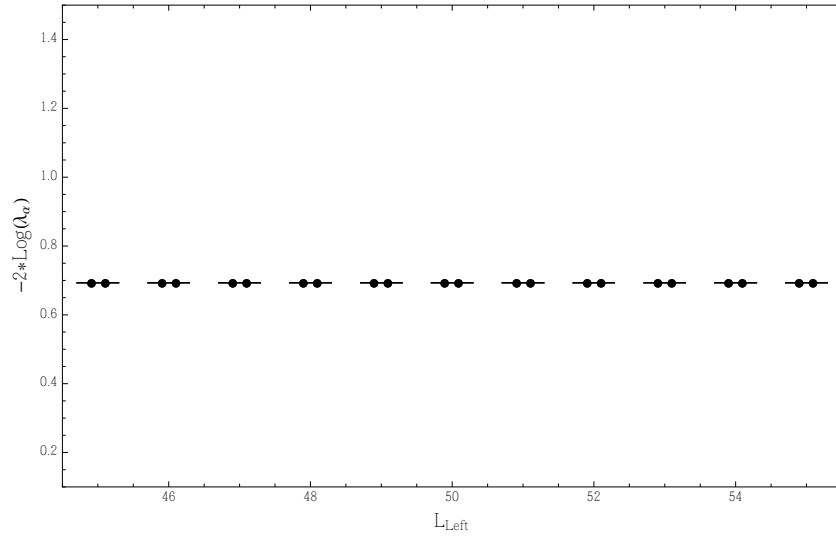


Figure 27: The entanglement spectrum is as expected doubly degenerated, which is a direct consequence of the AKLT singlet bounds.

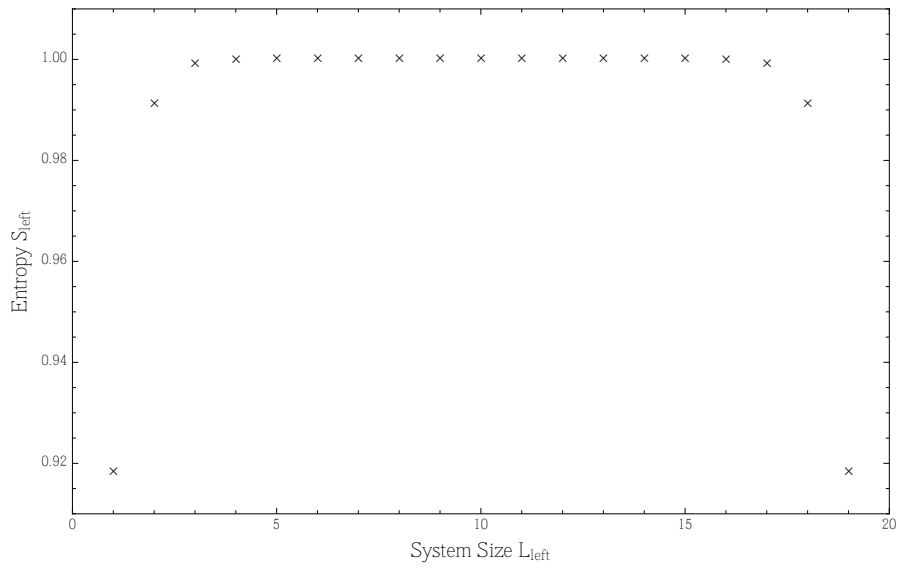


Figure 28: Plot of the entanglement entropy versus left system size L_{left} .

C.4 HEISENBERG MODEL

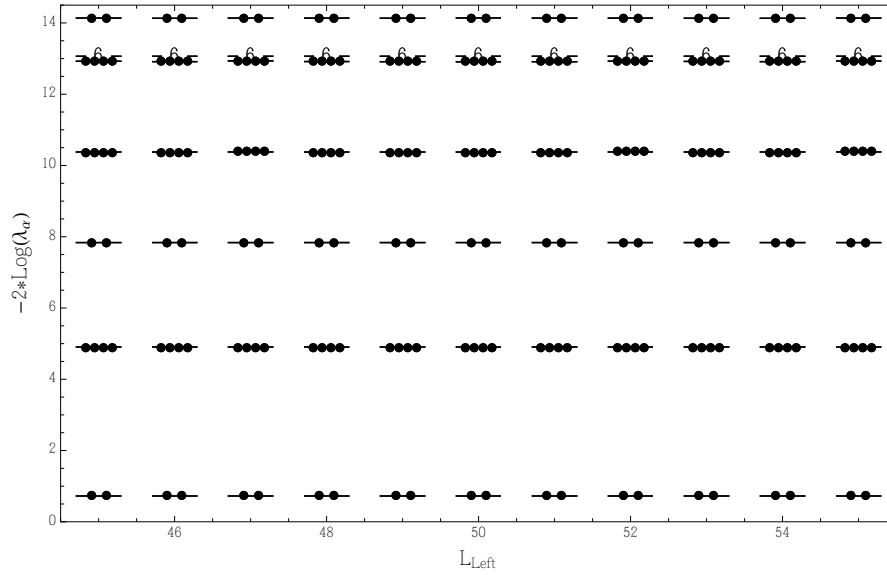


Figure 29: It is noticeable that the bounds of the Heisenberg spin-1 Hamiltonian obey a similar structure to the one of the AKLT states.

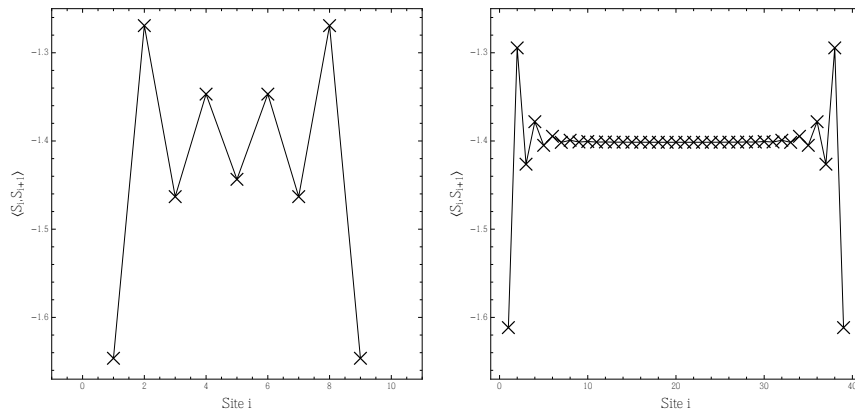


Figure 30: The effects of the open boundary conditions are clearly visible. For a comparable value, the energy per side has been recorded with a bond dimension of $m = 50$ for $L = 100$ sites, and the energy per site in the very center has been taken.

LIST OF FIGURES

Figure 1	Graphical Notation for Tensor Networks	6
Figure 2	Graphical representation of contraction 2.22.	6
Figure 3	Trace in Graphical Notation	7
Figure 4	Contraction Sequence Optimisation	7
Figure 5	AKLT MPS State	9
Figure 6	Sequential Singular Value Decomposition	10
Figure 7	Hamiltonian in MPO representation	12
Figure 8	Local Terms of the Hamiltonian	13
Figure 9	Canonical Gauge	15
Figure 10	Effective Hamiltonian	16
Figure 11	Norm Simplification due to Canonical Gauge	17
Figure 12	Left Side of the Effective Hamiltonian	18
Figure 13	Correlations in MPS Representation	20
Figure 14	Correlations with Canonical Basis	21
Figure 15	Ising Model: Majorana Modes	23
Figure 16	Ising Model: Energy, Analytical vs Numerical Values	24
Figure 17	Ising Model: Absolute Energy Deviation from Analytical Values	24
Figure 18	Ising Model: Absolute Magnetisation	25
Figure 19	Ising Model: Correlations vs Γ	26
Figure 20	Ising Model: Entanglement Entropy vs Site	27
Figure 21	BLBQ Model: Phase Chart	28
Figure 22	BLBQ Model: Hamiltonian in MPO Form	29
Figure 23	BLBQ Model: Entanglement Spectrum vs θ	32
Figure 24	Ising Model: Magnetisation for the Antiferromagnetic Case	45
Figure 25	Ising Model: Magnetisation Curve vs Γ - different m	46
Figure 26	Ising Model: Energy convergence vs m	46
Figure 27	AKLT Model: Entanglement Spectrum	47
Figure 28	AKLT Model: Entanglement Entropy	47
Figure 29	Heisenberg Model: Entanglement Spectrum	48
Figure 30	Heisenberg Model: Border Effects	48

LISTINGS

code/AKLT.m	34
code/EnergyOpti.m	37
code/EV_Obs.m	38
code/EV_Corr.m	39
code/HLStep.m	40
code/HRStep.m	40

BIBLIOGRAPHY

- [1] Ian Affleck, Tom Kennedy, Elliott H. Lieb, and Hal Tasaki. Rigorous results on valence-bond ground states in antiferromagnets. *Phys. Rev. Lett.*, 59:799–802, 1987.
- [2] Ralf Bulla, Theo A. Costi, and Thomas Pruschke. Numerical renormalization group method for quantum impurity systems. *Rev. Mod. Phys.*, 80:395–450, 2008.
- [3] S Ejima and H Fehske. DMRG analysis of the SDW-CDW crossover region in the 1D half-filled Hubbard-Holstein model. *Journal of Physics: Conference Series*, 200(1), 2010.
- [4] S. H. Glarum, S. Geschwind, K. M. Lee, M. L. Kaplan, and J. Michel. Observation of fractional spin $S=1/2$ on open ends of $S=1$ linear antiferromagnetic chains: Nonmagnetic doping. *Phys. Rev. Lett.*, 67:1614–1617, 1991.
- [5] G.Sardanashvily. Lectures on integrable Hamiltonian systems. 2013. arXiv:1303.5363v1.
- [6] M B Hastings. An area law for one-dimensional quantum systems. *Journal of Statistical Mechanics: Theory and Experiment*, 2007(08), 2007.
- [7] A. Kitaev and C. Laumann. Topological phases and quantum computation. 2009. arXiv:1303.5363v1.
- [8] A. Klümper. New Results for q-State Vertex Models and the Pure Biquadratic Spin-1 Hamiltonian. *EPL (Europhysics Letters)*, 9(8), 1989.
- [9] Fumiaki Morikoshi, Marcelo França Santos, and Vlatko Vedral. Accessibility of physical states and non-uniqueness of entanglement measure. *Journal of Physics A: Mathematical and General*, 37(22), 2004.
- [10] Román Orús. A Practical Introduction to Tensor Networks: Matrix Product States and Projected Entangled Pair States. 2013. arXiv:abs/1306.2164v1.
- [11] C. Pan and K. Sigmon. A Bottom-Up Inductive Proof of the Singular Value Decomposition. *SIAM Journal on Matrix Analysis and Applications*, 15(1), 1994.
- [12] Pierre Pfeuty. The One-Dimensional Ising model with a Transverse Field. 1970. *Ann.Phys.:Vol. 57*, pp.79-90.
- [13] Frank Pollmann, Ari M. Turner, Erez Berg, and Masaki Oshikawa. Entanglement spectrum of a topological phase in one dimension. *Phys. Rev. B*, 81:064439, 2010.
- [14] Frank Pollmann, Erez Berg, Ari M. Turner, and Masaki Oshikawa. Symmetry protection of topological phases in one-dimensional quantum spin systems. *Phys. Rev. B*, 85:075125, 2012.

- [15] Matteo Rizzi and Román Orús. Lecture notes: Entanglement in Many-Body Systems. 2013. Not published.
- [16] J Rodríguez-Laguna. Quantum wavefunction annealing of spin glasses on ladders. *Journal of Statistical Mechanics: Theory and Experiment*, 2007(05), 2007.
- [17] Ulrich Schollwöck. The density-matrix renormalization group in the age of matrix product states. 2013. arXiv:abs/1008.3477v2.
- [18] Tokuro Shimokawa and Hiroki Nakano. Frustration-Induced Ferrimagnetism in Heisenberg Spin Chains. *Journal of the Physical Society of Japan*, 80(12), 2011.
- [19] G. Vidal, J. I. Latorre, E. Rico, and A. Kitaev. Entanglement in Quantum Critical Phenomena. *Phys. Rev. Lett.*, 90:227902, 2003.
- [20] Steven R. White. Density-matrix algorithms for quantum renormalization groups. *Phys. Rev. B*, 48:10345, 1993.
- [21] Steven R. White and David A. Huse. Numerical renormalization-group study of low-lying eigenstates of the antiferromagnetic $S=1$ Heisenberg chain. *Phys. Rev. B*, 48:3844, 1993.
- [22] Kenneth G Wilson. The renormalization group: Critical phenomena and the Kondo problem. *Reviews of Modern Physics*, 47(4):773–840, 1975.

DECLARATION

Hiermit erkläre ich, dass ich diese Abschlussarbeit selbständig verfasst habe, keine anderen als die angegebenen Quellen und Hilfsmittel benutzt habe und alle Stellen, die wörtlich oder sinngemäß aus veröffentlichten Schriften entnommen wurden, als solche kenntlich gemacht habe. Darüber hinaus erkläre ich, dass diese Abschlussarbeit nicht, auch nicht auszugsweise, im Rahmen einer nichtbestandenenen Prüfung an dieser oder einer anderen Hochschule eingereicht wurde.

I hereby declare that this thesis and the work reported herein was composed by and originated from me. Information derived from the published and unpublished work of others has been acknowledged in the text and references are given in the list of sources. Furthermore I declare, that this thesis has not been submitted at any university within the scope of a failed exam.

Mainz, April 7, 2014